SEASONAL VARIATION OF INFILTRATION RATES THROUGH POND BED IN A MANAGED AQUIFER RECHARGE SYSTEM

A Thesis

by

SAYANTAN SAMANTA

Submitted to the Office of Graduate and Professional Studies of
Texas A&M University
in partial fulfillment of the requirements for the degree of

MASTER OF SCIENCE

Chair of Committee,	Clyde L. Munster
Co-Chair of Committee,	Zhuping Sheng
Committee Member,	Peter Knappett
Head of Department,	R. Karthikeyan

August 2018

Major Subject: Water Management and Hydrological Science

ABSTRACT

Managed Aquifer Recharge (MAR) has become a powerful tool for increasing water supplies around the world. The Torreele Waste Water Treatment Plant (TWWTP) in Belgium uses MAR to recharge the aquifer with treated wastewater in order to sustain the potable water supply on the Belgian coast. The treated water from the TWWTP is transported to two infiltration ponds where it is recharged into a 30m deep phreatic aquifer by the natural process of infiltration under gravity. One of the challenges of the MAR facility is the reduced infiltration rates during the winter season when pond water temperatures vary from 4 °C to 10 °C. The infiltration capacity is approximately 50.5 to 100 % higher in summer as compared to that in winter.

Several factors including pumping rate around ponds, natural recharge, tidal influences of the North Sea and pond-water temperature were identified as potential causes for the variation of recharge rate. This study involves the identification of the predominant factor influencing the rate of infiltration through the pond bed. Correlation statistics and linear regression analysis have been used to determine the sensitivity of infiltration rate to the aforementioned factors. Results showed that water temperature has the maximum impact on infiltration rate. Cyclic variations in water viscosity, occurring as a result of seasonal temperature changes, influence the saturated hydraulic conductivity of the pond bed. A lower infiltration rate through the pond bed is observed during the winter months due to increased viscosity, which results in a decline in saturated hydraulic conductivity of the sandy soil. Temporal changes in the vertical hydraulic gradient is another factor that could alter infiltration rate as the pumping rate around the pond causes fluctuations in the groundwater level.

Two groundwater flow models have been developed in visual MODFLOW to simulate the water movement under the pond bed. The response of groundwater levels to artificial recharge

from the pond under hypothetical scenarios for summer and winter months are assessed to obtain the differences in flux and track the effects of variation of hydraulic conductivity during the two seasons. It is observed from the models that higher leakance through infiltration pond bed in summer corresponds to the reduced heads in the monitoring wells and lower leakance corresponds to the higher heads, hence proving the impact of temperature influenced hydraulic conductivity in variation of infiltration rate.

ACKNOWLEDGEMENTS

I am using this opportunity to express my gratitude to everyone who supported me throughout the course of my research. I am thankful to my committee co-chairs, Dr. Sheng and Dr. Munster for providing me with this opportunity to work on this enlightening project. I would also like to thank Dr. Knappett for his support and guidance during the course of this study.

This thesis would have been impossible without the support of Mr. Van Houte, who provided us with all the information from the Torreele Managed Aquifer Facility.

I place on record, my sincere thank you to my friends for the continuous encouragement.

Finally, I thank my parents and Prajata for the unceasing encouragement, support and attention.

CONTRIBUTORS AND FUNDING SOURCES

Contributors

This work was supported by a thesis committee consisting of Dr. Clyde L. Munster and Dr. Zhuping Sheng of Biological and Agricultural Engineering Department and Dr. Peter Knappett of the Department of Geology and Geophysics.

Data used for analysis in Chapter II through IV was provided by Mr. Emmanuel Van Houte of IWVA, Belgium (Intercommunal Water Company of Veurne-Ambacht).

All other work conducted for the thesis was completed by the student independently.

Funding Sources

This work was made possible in part by the Water Seed Grant: Creation and Deployment of Water-Use Efficient Technology Platforms Program of Texas A&M AgriLife Research, the Texas A&M AgriLife Extension Service and the Texas A&M Engineering Experiment Station (TEES), US Department of Agriculture-National Institute of Food and Agriculture Hatch Project (TEX0-1-9448) via Texas A&M AgriLife Research.

Graduate study was partly supported by a scholarship from the Department of Water Management and Hydrological Science.

NOMENCLATURE

MAR	Managed Aquifer Recharge
TWWTP	Torreele Wastewater Treatment Plant
IR	Infiltration Rate
mTAW	Belgian National Reference Level for surface elevation (2.36 m below mean sea level)
DJF	December, January and February
MAM	March, April and May
JJA	June, July and August
SON	September, October and November

TABLE OF CONTENTS

Page

LIST OF FIGURES

Page

LIST OF TABLES

Page

CHAPTER I

INTRODUCTION

1.1 Background

Managed Aquifer Recharge (MAR) is a relatively new method to increase potable water supplies. MAR provides a sustainable solution to increasing water demand, without compromising the water quality. This process also helps to maintain groundwater levels and act as an effective barrier to saltwater intrusion in coastal aquifers (Todd, 1974). Groundwater extraction in St. André, Belgium, started in 1947 with the primary purpose of supplying drinking water (Vandenbohede et al., 2008b). In 1967, a second pumping well network was set up, increasing the groundwater extraction rate to 2 million m^3 $year^{-1}$. This high extraction rate in the coastal aquifer caused a substantial decline in the water table, followed by saltwater intrusion. To partially restore the fresh groundwater table, extraction in the region had to be reduced. The decision to artificially recharge the dune aquifer was made to remediate this problem. The year 2002 marked the start of artificial recharge operations in Torreele, Belgium.

Managed aquifer recharge has become a very popular strategy to deal with surface and groundwater problems (Sheng & Zhao, 2015), by improving groundwater quality and securing water supplies. An illustration of a Managed Aquifer Recharge system is shown in Figure 1. MAR is a comprehensive system consisting of seven components: (1) source water, (2) pretreatment, (3) recharge facilities, (4) storage space (suitable aquifer), (5) recovery facilities, (6) post-treatment, and (7) end-use (Sheng, 2005) (NRMMC, 2008). The main objective of the Torreele MAR facility is to meet the water demands of the surrounding area, replenish the overexploited aquifer and restore the groundwater table in the unconfined dune aquifer (Vandenbohede et al., 2008b).

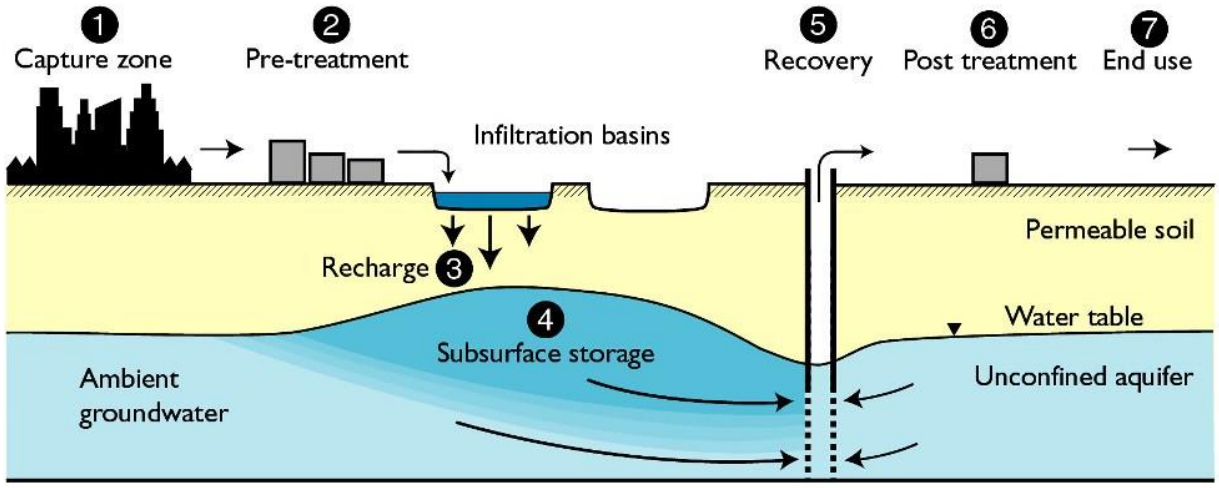

Figure 1. Managed Aquifer Recharged in a confined aquifer (NRMMC, 2008)

1.2 Problem statement

Infiltration rate (IR) is the most important parameter controlling recharge in the Torreele Managed Aquifer Recharge facility. A higher infiltration rate through the pond bed signifies better recharge capacity and in turn providing groundwater extraction potential. However, data collected from this facility indicates that the infiltration capacity is lower in the winter and higher in the summer. The magnitude of infiltration rates during the winter season reduces by 50-100 % (Vandenbohede & Lebbe, 2012) when compared to the infiltration capacity during summer. As a result, water yields from the MAR system are lower during the winter.

1.3 Objectives

This study used observed data from Torreele, Belgium to understand the water movement below the infiltration basin and the seasonal variation of hydraulic conductivity under different climatic conditions. Two groundwater flow models were developed to identify variations in the average linear flow velocities of water with slight variations in hydraulic conductivity occurring

over time. The key task here is to identify the primary cause for the variation of recharge rates in the area. The infiltration ponds are directly connected to the groundwater, therefore there is no unsaturated zone between the ponds and the groundwater table, and hence there is no possibility of air entrapment. In this study, the factors that have been studied are (1) changes in hydraulic head due to natural recharge, (2) tidal effects, (3) temperature-induced changes to water viscosity, and (4) aquifer drawdown owing to pumping by the surrounding production wells.

The objectives of this study are to:

(1) Understand the overall flow process in the Torreele MAR facility,

(2) Identify possible factors that influence the variation in infiltration capacity in this site

(3) Develop a relationship between the dominant factor and infiltration rates

(4) Develop MODFLOW models to simulate water movements below the ponds and assess hypothetical scenarios for summer and winter to assess flux and flow velocity during the two seasons.

1.4 Study Area

1.4.1 Torreele Wastewater Treatment Plant

The Torreele Wastewater Treatment Plant (TWWTP) is located 4 km inland from the coast of North Sea. It started operating in July 2002 following numerous pilot (Van Houtte & Verbauwhede, 2012). Figure 2 shows that steps involved in the filtration process.

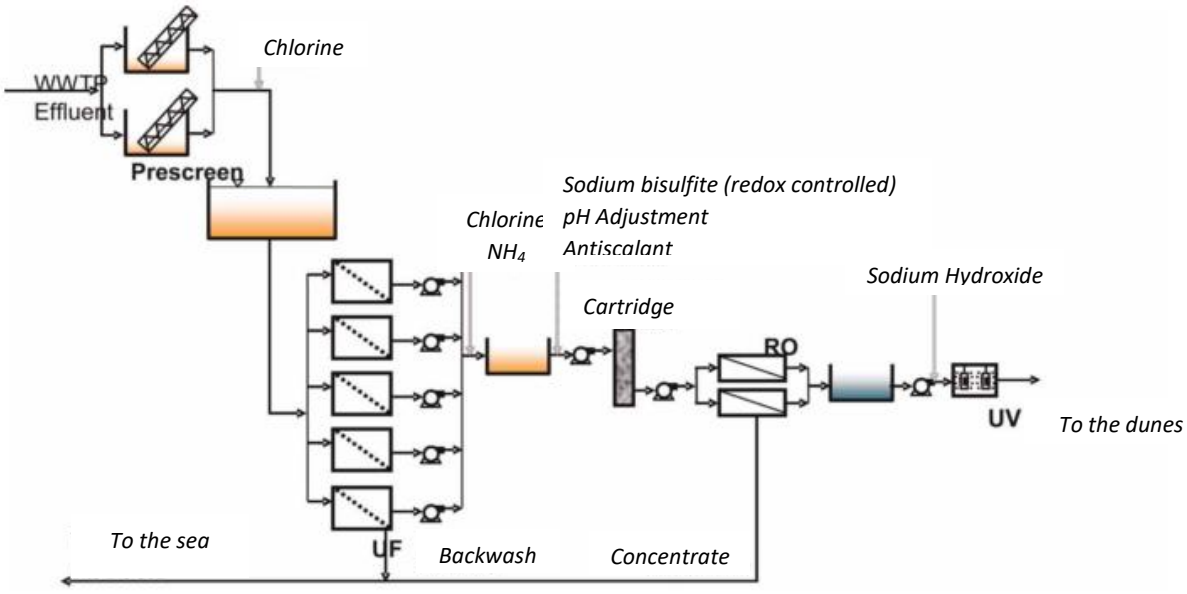

Figure 2. Process Scheme of Torreele Wastewater Treatment Plant *(Van Houtte & Verbauwhede, 2012)*

Secondary wastewater generated by surrounding urban areas is the source water for this treatment facility (Pantoula, 2012). The first step in the process is passing the water through prescreens that remove bigger particles. It is then passed through a chlorine tank followed by chlorine resistant ultrafiltration (UF) membranes having a maximum pore size of 0.1 μm. This method helps in removing suspended solids and bacteria. Next, the water is passed through a cartridge filter followed by a two-stage reverse osmosis (RO) membrane sets. This step removes microbial, chemical contamination and dissolved solids. The water is then dosed with sodium hydroxide and ultraviolet (UV) disinfection is performed on it. This treated wastewater is the source water for the Torreele Managed Aquifer Recharge (MAR) facility.

1.4.2 Torreele Managed Aquifer Recharge Facility

The MAR facility is located on the west coast of Belgium, close to the French-Belgium border (Figure 3). The recharge pond is located on the dunes of the western Belgian coastal plain. The dune extends inland by 2 km to 2.5 km and has a surface elevation ranging from 6 mTAW to 35 mTAW (mTAW is the reference level corresponding to the mean low tide level, calculated as 2.36 m below mean sea level; mTAW is a standard Belgian reference).

The mean thickness of the Quaternary phreatic aquifer under the entire region is 30m. The confining layer of this aquifer is a 100m thick clay layer, which is of the Eocene age and is considered impermeable in this study. The upper part of the aquifer consists of yellow Aeolian dune sands having considerable amounts of organic matter in it. A larger part of the aquifer is comprised of fine medium sand with occasional presence of silty and fine clayey sand lenses. The lower part of the aquifer consists of medium to coarse-medium sand pertaining to Eemian age (Vandenbohede et al., 2008b).

The Torreele Wastewater Treatment Plant (TWWTP) provides the reclaimed wastewater (source water) to this MAR facility through a 2.5 km long pipeline from the treatment plant (pretreatment) to the coastal recharge site. The treated wastewater (source water) supplies an artificial infiltration pond (recharge method) with a surface area of 18,200 m^2 at St-Andre, Belgium. The infiltration pond recharges an unconfined sandy dune aquifer (storage space) and water is then recovered from this aquifer using 137 wells (recovery facilities) which surround the pond. The recovered water is then used for municipal water supplies (end use) after aeration step, rapid sand filtration and UV disinfection (post-treatment) (Van Houtte & Verbauwhede, 2012). Figure 4 shows a schematic diagram of the processes involved in the Torreele MAR facility.

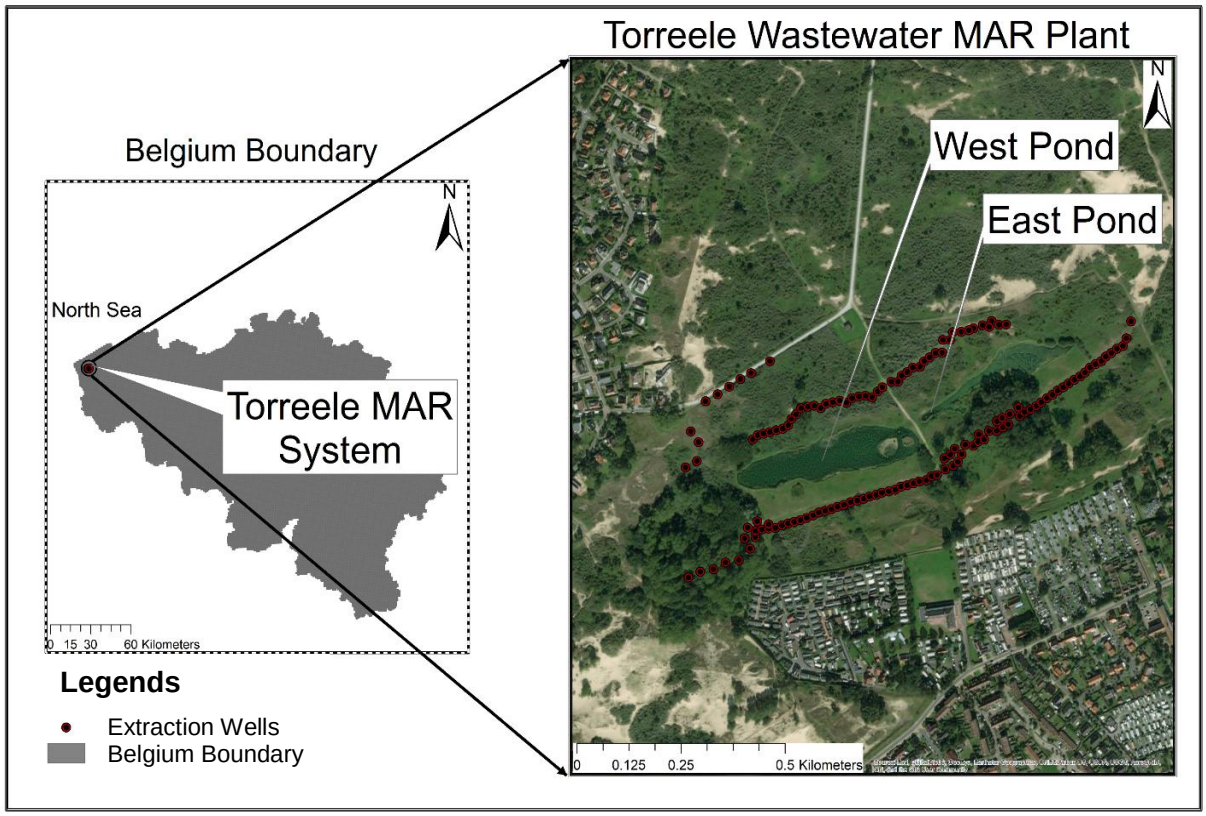

Figure 3. Torreele Managed Aquifer Recharge Facility

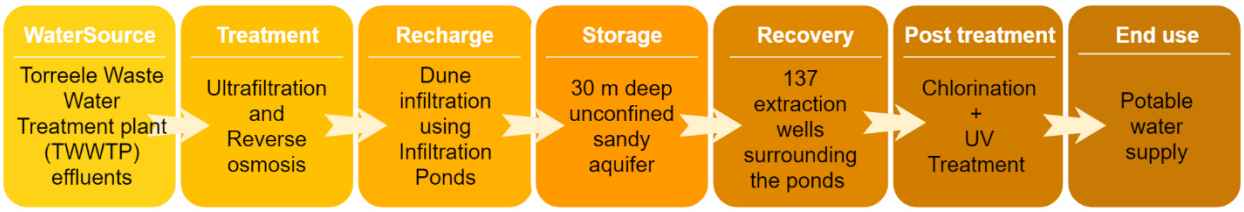

Figure 4. Process of Torreele Managed Aquifer Recharge Facility

Figure 5 shows the location of the monitoring wells. The wells are represented as WP, which is the abbreviation of Dutch words “Waarneming Putten”, meaning observation wells. The convention used for numbering the wells are shown in figure 6. All monitoring wells have a series of 4 levels of well with screen openings at different depths. The level 1 wells have screens at -20 mTAW, which are the deepest wells and level 4 wells are the shallowest wells having screens at -

3.55 mTAW. The ground elevation around the pond is 7.1 mTAW and the pond bed elevation is 6.2 mTAW.

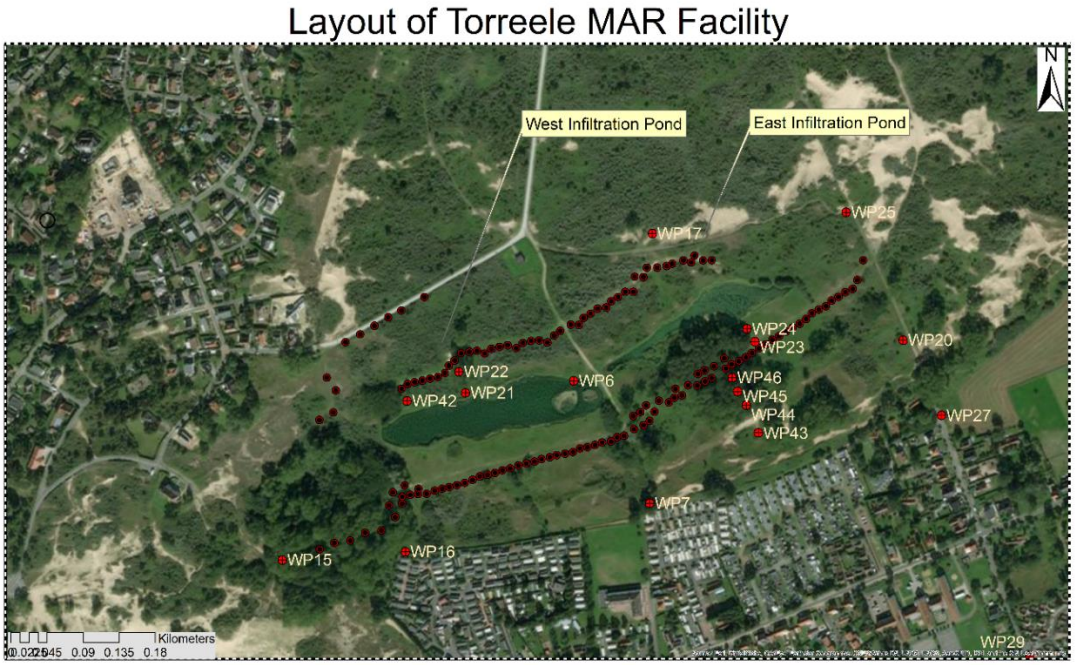

Figure 5. Location of monitoring wells at the Torreele MAR site

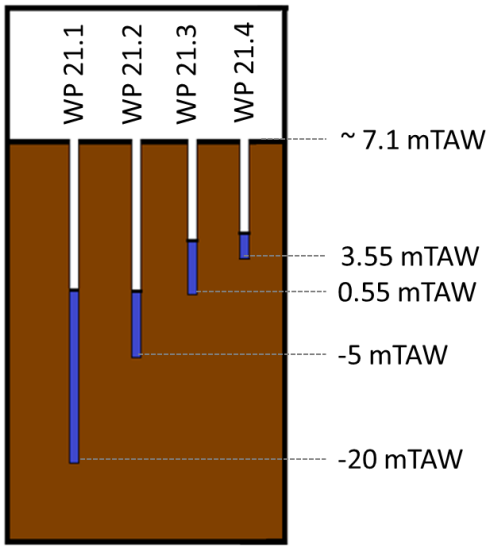

Figure 6. Schematic reference of well screen depths at Torreele MAR site

CHAPTER II

TORREELE DATA ANALYSIS

2.1 Prediction of temperature of water at infiltration ponds during periods of missing record

Data obtained from the Torreele MAR facility had periods of missing data. To combat this problem, Genetic Programming (GP) has been employed. GP is a form of evolutionary algorithm, which is a component of machine learning. GP is a powerful tool, which employs non-linear regression to develop a relationship between variables with very little domain knowledge (Koza, 1994).

The statistical indices used for evaluating the efficiency of the model are coefficient of determination (R^2) (equation 1) and Nash-Sutcliffe Efficiency (NSE) (equation 2)

$$R^2 = \frac{\left(n(\sum {Y_i}^{obs}.{Y_i}^{sim})-(\sum {Y_i}^{obs})(\sum {Y_i}^{sim})\right)^2}{\left[n\sum {Y_i}^{obs^2}-\left(\sum {Y_i}^{obs}\right)^2\right]\left[\left(n\sum {Y_i}^{sim^2}-\left(\sum {Y_i}^{sim}\right)^2\right)\right]} \quad 1$$

Where, ${Y_i}^{obs}$ is the i[th]-observed value and ${Y_i}^{sim}$ is the i[th]-simulated value. R^2 is the measure of collinearity and the range of R^2 is from 0 to 1, 0 being least collinear and 1 being exactly identical.

$$NSE = 1 - \left[\frac{\sum_{i=1}^{n}\left({Y_i}^{obs}-{Y_i}^{sim}\right)^2}{\sum_{i=1}^{n}\left({Y_i}^{obs}-Y^{mean}\right)^2}\right] \quad 2$$

Where, Y^{mean} is the mean of observed data. NSE indicates the goodness of fit of the plot between observed and simulated data to the 1:1 line. The range of NSE is -∞ to 1, 1 being the optimal value (Moriasi et al., 2007).

Temperature data of water in the infiltration ponds are available from January 2014 to June 2015 and from April to June 2016. For the missing period, Genetic Programming (GP) has been

employed to develop a non-linear relationship between minimum and maximum air temperatures with water temperature in the infiltration ponds. Figure 5 shows the equation tree consisting of numeric operators and 2 variables, X1 and X2. X1 is the minimum air temperature, X2 is the maximum air temperature and Y is pond water temperature.

The model has been developed over a period of January – December 2014 and has been validated over January – June 2015. Table 1 shows the development and validation statistics. The results obtained by this method shows a fair agreement (Figure 7). The correlation between observed and simulated pond water temperature is 0.93 and that during validation is 0.89. The equation tree (figure 32) has been used to predict pond water temperature until December 2016. The complete equation (equation 24) can be found in Appendix A.

Table 1. Statistics of agreement between simulated and observed pond water temperatures using Genetic Programming

	R^2	*NSE*
Calibration	0.93	0.86
Validation	0.89	0.80

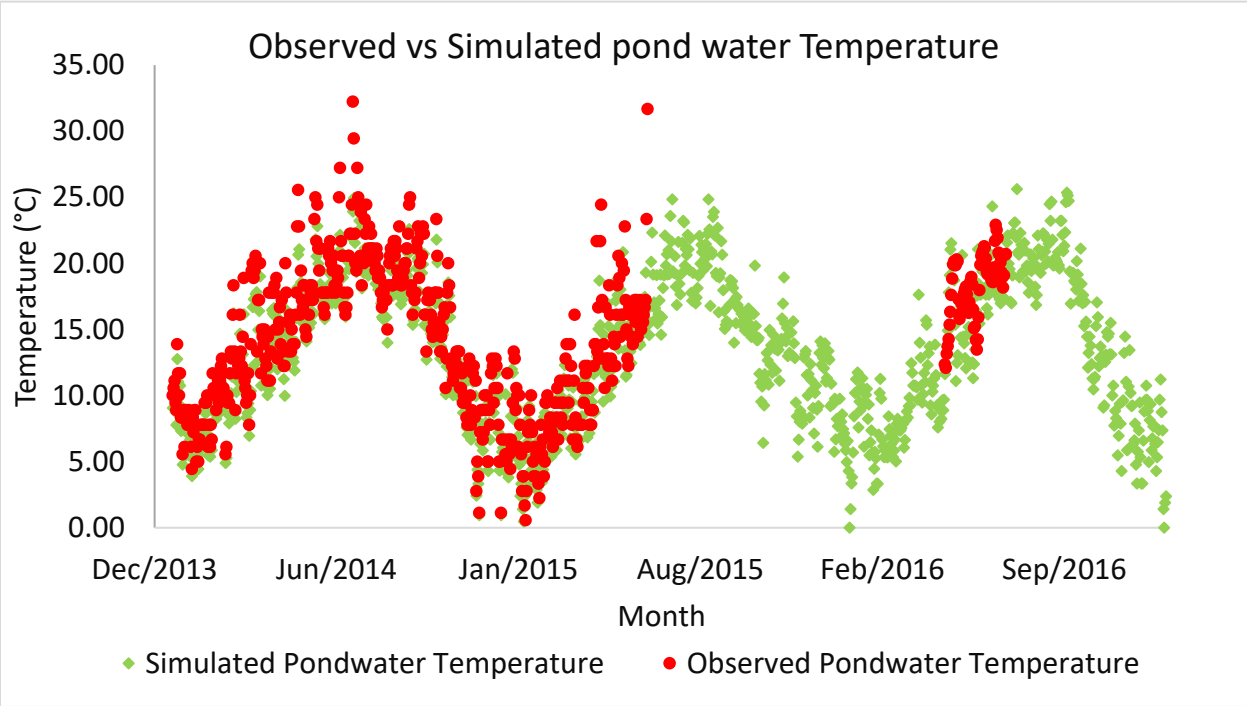

Figure 7. Observed pond water temperature vs simulated pond water temperature using Genetic Programming

2.2 Analysis of monthly inflow to ponds

A seasonal analysis was performed on the amount of water supplied to the infiltration ponds from the TWTTP (inflow) for a period of 12 years. The seasons were divided as follows: (1) December, January and February (DJF) for winter, (2) March, April and May (MAM) for spring, (3) June, July and August (JJA) for summer, and (4) September, October and November (SON) for autumn.

The highest inflow to the ponds is observed in the summer season (JJA) and the lowest is observed in the winter season (DJF) (figure 8). This seasonal variation in inflow justifies the problem statement and provides the prime motivation for this study. The study area is near the

coast of the North Sea and experiences a high tourist population during the summer season increasing the water demand and increasing the need to pump more.

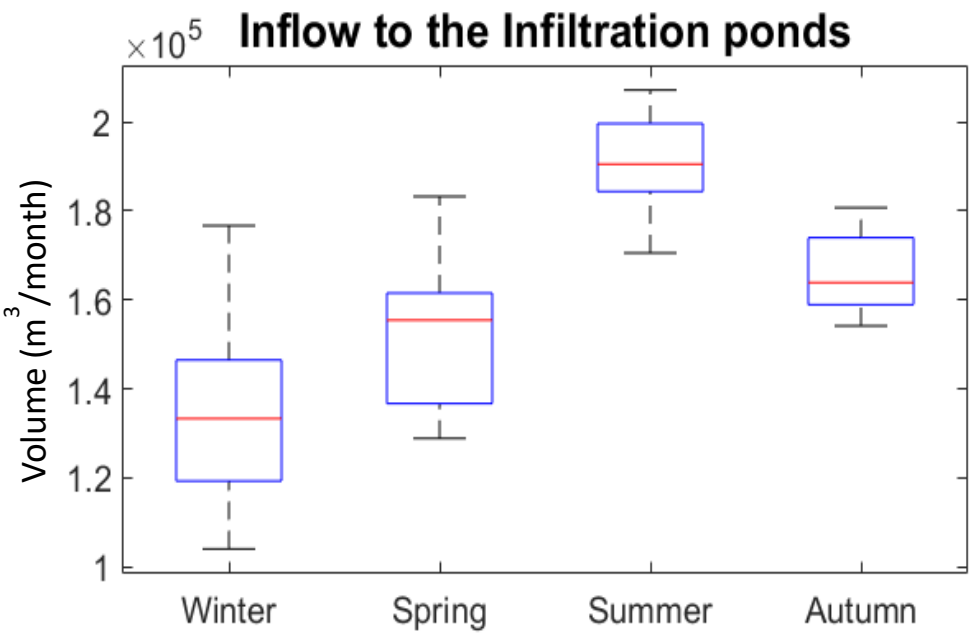

Figure 8: Box plot of monthly inflow to the ponds

According to Pantoula (2012), the infiltration limit is 2.5 million m^3 $year^{-1}$ and so is the extraction limit. In addition to this, 1.7 million m^3 $year^{-1}$ of natural dune water can be pumped. Hence, the pumping rate is always higher than the infiltration rate. The idea of the MAR system is to develop a sustainable system by using less of existing natural water in the aquifer and more of the recharged water.

2.3 Groundwater flow analysis

Contours of groundwater elevations have been developed using data obtained from monitoring wells around the pond at elevations -5 mTAW and -20 mTAW. Four days have been selected to monitor the contours, two representing winter (01/19/2015 and 01/11/2016) and two

representing summer (07/13/2015 and 07/19/2016). The contours help in visualizing the groundwater elevations as well as the direction of water flow. The flow of groundwater occurs in two distinct directions, i.e. radially outwards from the infiltration ponds to the pumping wells and radially inwards from the area outside the pumping wells towards the pumping wells. This happens because the pumping rate is usually higher than the rate of recharge through the ponds and existing natural water in the dunes contribute to the high extraction volume. For this reason, contour development has been presented in two phases: (1) a small region near the infiltration ponds influenced only the artificial recharge and (2) a larger region showing the inward radial flow of natural groundwater towards the pumping wells.

2.3.1 Flow analysis of artificially recharged water

The infiltration ponds are the primary source of water in the area between the ponds and pumping wells. The pumping wells create a barrier to the flow of water around the ponds. Contours have been developed at a depth of -5 mTAW, using groundwater elevations at the Level 2 wells. Groundwater elevations represent the horizontal flow directions. The flow direction is perpendicular to the contour lines.

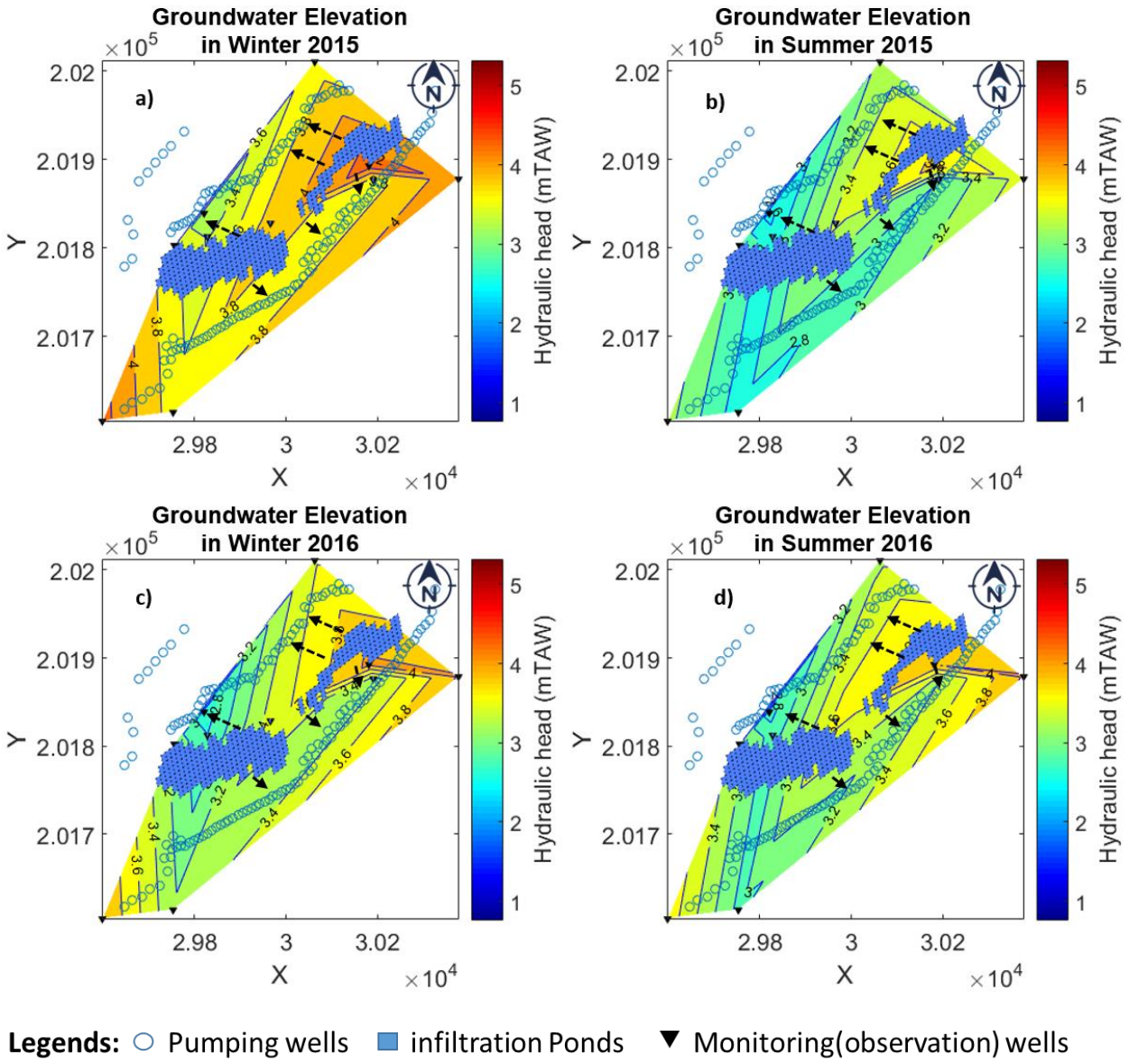

Figure 9. Contour of hydraulic head near the infiltration ponds at -5 mTAW (Level 2 monitoring wells) during: a) Winter 2015 (01/09/2015), b) Summer 2015 (07/13/2015), c) Winter 2016 (01/11/2016) and, d) Summer 2016 (07/19/2016)

The flow in this region is outwards from the ponds to the pumping wells. The variation of groundwater elevations is visible between the summer and winter seasons in figure 9. The contour lines have higher values in winter 2015 and 2016 (figure 9.a and 9.c). Heads are lower during

summer 2015 and 2016 (figure 9.b and 9.d) indicating a higher vertical gradient between the pond and the aquifer, thereby increasing the flow rate. The direction of flow does not change over time. However, the horizontal gradient is observed to increase in summer in the northern parts of the infiltration ponds. This also suggests that flow rate is higher in summer.

2.3.2 Flow analysis of natural groundwater

Groundwater level contours at a depth of -5 mTAW (Level 2 monitoring wells) are shown in figure 10. It can be observed from the contours that the hydraulic heads around the pumping wells are higher during the winters (figure 10.a, 10.c, 11.a and 11.c) and lower during the summers (figure 10.b, 10.d, 11.b and 11.d). The same effect can be observed in groundwater elevations at Level 1 monitoring wells located at -20 mTAW elevation. The groundwater flow is radially inwards towards the location of the pumping wells.

The average horizontal gradient in winter is 1.35E-03 whereas that in summer is 1.38E-03 for the Level 2 wells. In the Level 1 wells, the average horizontal gradient in winter is 1.13E-03 whereas that in summer is 1.35E-03. This indicates higher flows from the dunes to the pumping wells in summer than in winter.

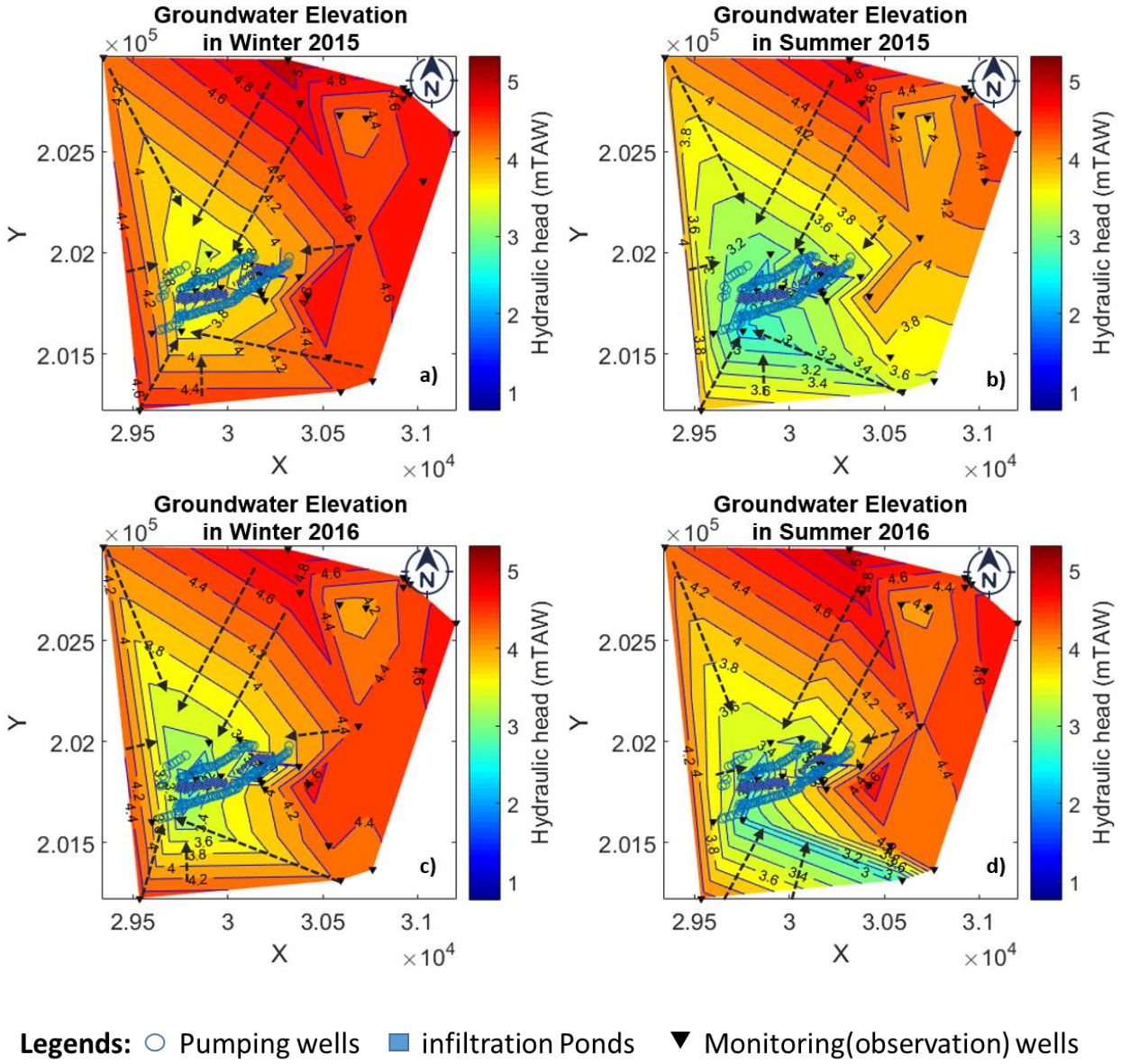

Figure 10. Contour of hydraulic head at -5 mTAW (Level 2 monitoring wells) around the pumping wells during: a) Winter 2015 (01/09/2015), b) Summer 2015 (07/13/2015), c) Winter 2016 (01/11/2016) and, d) Summer 2016 (07/19/2016)

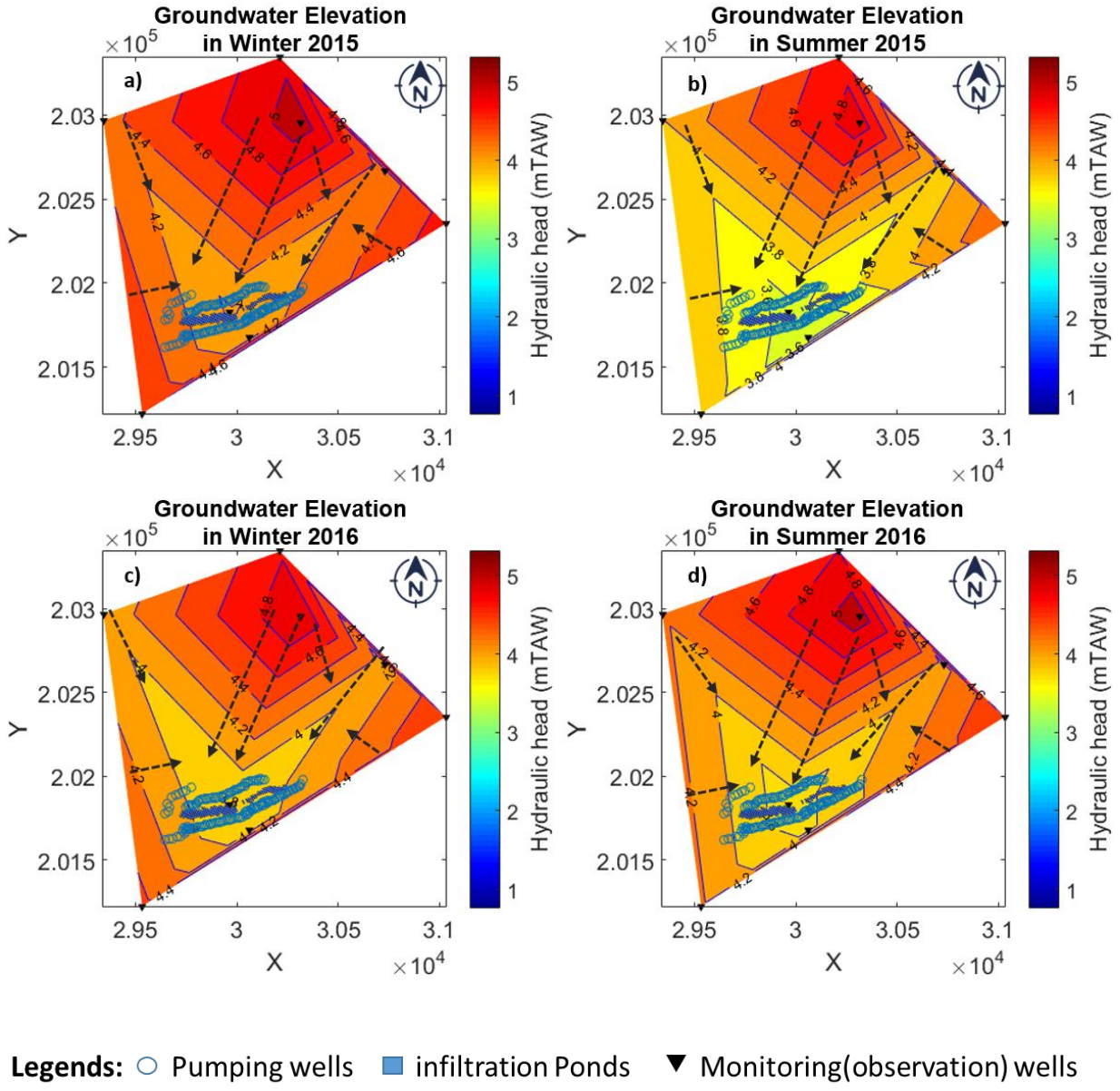

Figure 11. Contour of hydraulic head at -20 mTAW (Level 1 monitoring wells) around the pumping wells during: a) Winter 2015 (01/09/2015), b) Summer 2015 (07/13/2015), c) Winter 2016 (01/11/2016) and, d) Summer 2016 (07/19/2016)

2.4 Regional vertical hydraulic gradient analysis

Vertical hydraulic gradient provides an estimate of the vertical flow rate as well as the direction of flow (upward or downward). Vertical gradients are calculated using heads at

elevations 3.55 mTAW (approximately 3 m below the surface), 0.55 mTAW (approx. 6 m below the surface) and -5 mTAW (approx. 11.5 m below the surface) at well series WP 21, 22, 23 and 24 surrounding the infiltration ponds. Analysis has been done on the average heads for the summer months (JJA) and the winter months (DJF) for 2015 and 2016. The variation of hydraulic heads with different seasons is also reflected on the vertical hydraulic gradient. It is observed that the vertical gradient is usually higher in summer and lower in winter as seen in figures 12 and 13.

Vertical hydraulic gradient is calculated as (equation 3):

$$i = \frac{dh}{dz} \qquad 3$$

Where, *i* is vertical hydraulic gradient (-), *dh* is change of head (m) and *dz (m)* is change in elevation.

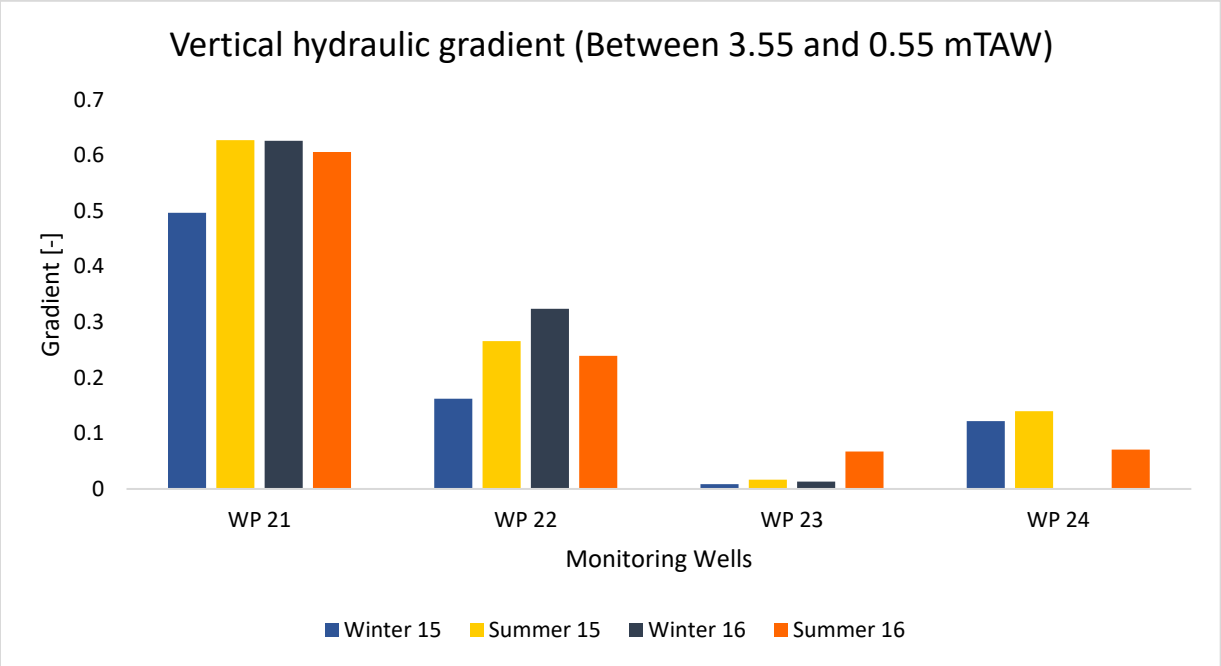

Figure 12: Vertical hydraulic gradient in Well series 21, 22, 23 and 24 for 2015-2016 period between Level 4 (3.55 mTAW) and Level 3 (0.55 mTAW) wells

Between 3.55 mTAW and 0.55 mTAW elevation, the hydraulic gradient is higher in summer than that in winter for the WP 21, 23 and 24 monitoring wells. However, at WP 22, the

winter of 2016 showed a higher gradient than the summer gradients. This may be attributed to a less permeable soil lens present in the area. WP 21 shows very high hydraulic gradients in both summer and winter, suggesting the presence of a less permeable lens in the area between 3.55 and 0.55 mTAW in the northern side of the west pond. The occurrence of a shallow low-permeable layer under the western pond is also mentioned by Vandenbohede et al. (2008a) between 3.55 and 0.55 mTAW. However, the lateral extent of the layer in unknown.

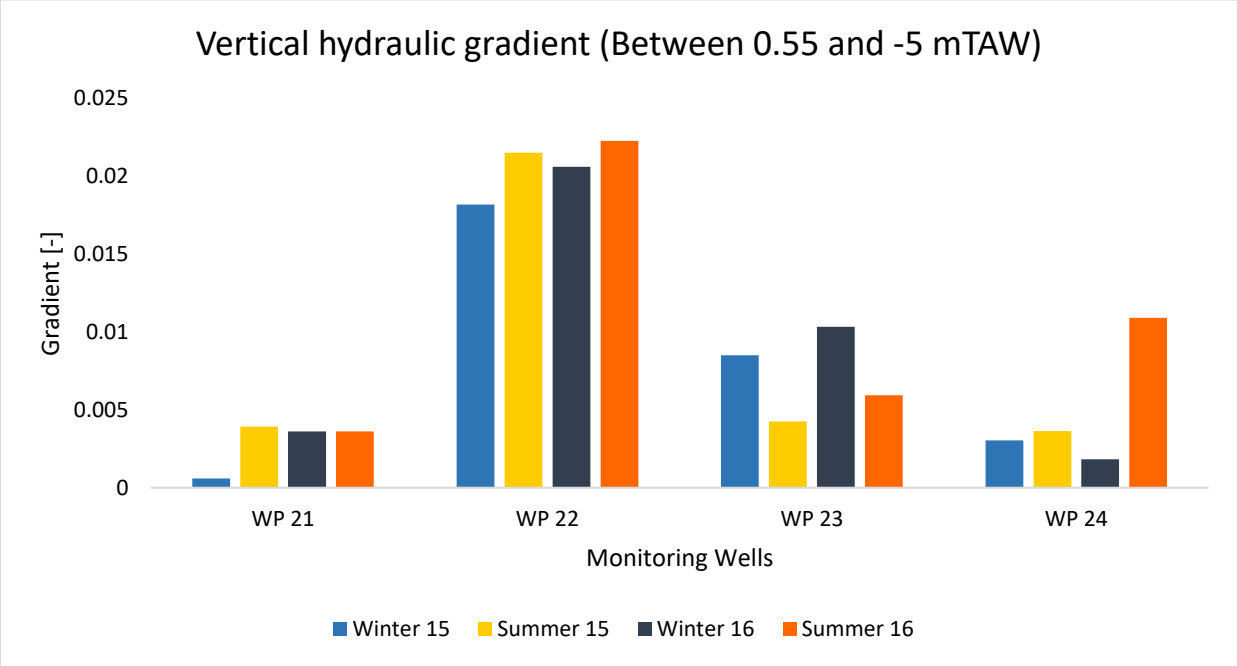

Figure 13. Vertical hydraulic gradient in Well series 21, 22, 23 and 24 for 2015-2016 period between Level 3 (0.55 mTAW) and Level 2 (-5 mTAW) wells

Between 0.55 mTAW and -5 mTAW elevation, there is not much variation in gradients. The lower part of the aquifer has lower hydraulic conductivity (Vandenbohede et al., 2008b). From the regional groundwater model and the existing local groundwater model (Vandenbohede & Houtte, 2012), it is inferred that the hydraulic conductivity is approximately 20 m day^{-1} at the top

of the aquifer and 1 m day^{-1} at the bottom. In WP 23, the summer gradients are higher than the winter gradients. This occurrence is probably due to the high anisotropy in the region.

2.4 Vertical gradient analysis with reference to infiltration ponds

WP 6.2 is assumed to reflect the conditions exactly underneath the ponds as it is located centrally between the two ponds. Vertical hydraulic gradient has been calculated between WP 6.2 and the pond bed to observe the variation of vertical gradient between summer and winter. Figure 14 shows that the gradients are higher for summer of 2015 and 2016 in comparison to the winter of 2015 and 2016. This also suggests that the rate of infiltration through pond bed is higher in summer as compared to that in winter.

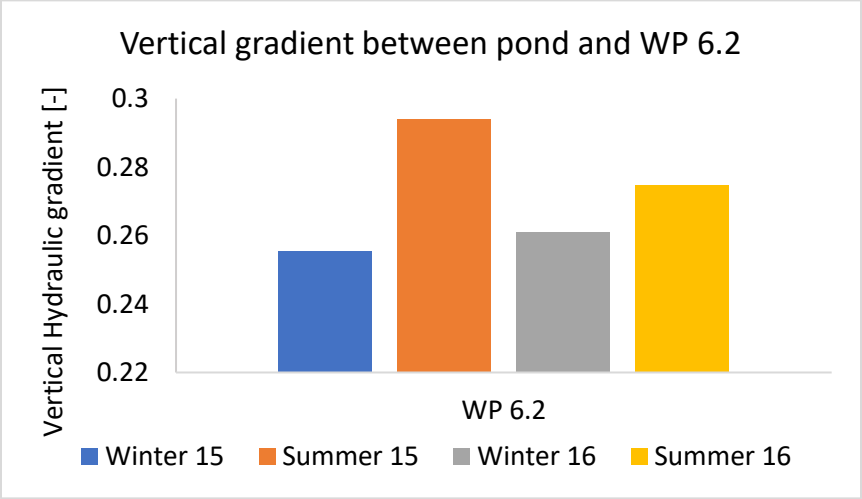

Figure 14. Vertical hydraulic gradient between WP 6.2 and pond bed

2.5 Discussion

According to Darcy's Law (equation 4),

$$q = K \times i \quad (4)$$

Where, *q* is specific discharge (m day^{-1}), *K* is hydraulic conductivity (m day^{-1}) and *i* is hydraulic gradient (-).

Assuming hydraulic conductivity does not change over time,

$$q \propto i \quad (5)$$

Hence, the rate of vertical flow is directly proportional to the change in vertical hydraulic gradient. During the summer season, a lowering in hydraulic head is observed followed by an increase in vertical gradient. As a result, the vertical flow velocity is expected to be higher in summer. During the winter, the reverse phenomenon is observed. As the hydraulic head rises, the vertical gradient lowers and flow velocity reduces. It is seen from the vertical hydraulic gradients at WP 6.2 that the hydraulic gradient reduces considerable in winter as compared to that in summer.

The average reduction in regional vertical hydraulic gradient in winter as compared to summer is 32 % from 3.55 to 0.55 mTAW depth and 4 % from 0.55 to -5 mTAW. However, Vandenbohede & Houtte (2012) reports that the reduction of infiltration capacity in winter is as high as 50 – 100 %. Thus, the variation in vertical hydraulic gradient alone does not contribute to the overall fluctuation of infiltration rates. Hence, the assumption that hydraulic conductivity is constant over time does not stand valid and it is essential to take into account the variability of hydraulic conductivity as well.

CHAPTER III

FACTORS INFLUENCING INFILTRATION RATE

3.1 Introduction

The variation of vertical flow velocity of groundwater may occur as a result of changes in aquifer properties such as lower hydraulic gradient, reduced hydraulic conductivity of aquifer media and reduced leakance through pond bed occurring as a result of reduced conductivity of the bed during the winter. Previous studies show that there are numerous factors affecting infiltration rates. Lin et al. (2003) state that possible factors responsible for the reduction in infiltration rate are physical clogging, biological clogging, entrapped air, dispersion or the swelling of clay. Low temperatures are also effective at reducing hydraulic conductivity of the soil media. They studied the impact of temperature in the variation of infiltration rate through a natural porous media and found that viscosity was not the only temperature dependent factor that controlled IR variation. They opened the room for more possible solutions to this phenomenon.

Loizeau et al. (2017) have studied the combined involvement of water temperature and air entrapment on infiltration rate variations and reported that the effect of temperature and air entrapment are of equal magnitude. Constantz & Murphy (1991) studied the temperature dependence of ponded infiltration and found that there is a strong influence of temperature which lead to the study of diurnal variations in temperature of stream water and its effect on streambed seepage in a losing stream (Constantz, 1998). It is seen that the hydraulic conductivity of soil is influenced by temperature causing a reduction in afternoon streamflow. Vandenbohede & Houtte (2012) have also studied the infiltration rate in the Belgium MAR site and inferred that temperature influences residence times of infiltrated water. The found that a combined effect of variation in

infiltration, extraction rates and residence time of infiltrated water contributes to the seasonal variability of infiltration rate from the ponds.

3.2 Methodology

Infiltration rate through pond bed was calculated by equation 6, developed using the water budget equation.

$$q = \frac{Q}{A} + \frac{dH}{dt} - E + P \quad (6)$$

Where, q is the infiltration rate (m/day), Q is the measured inflow to the pond (m^3 day^{-1}), A is the surface area of the pond (m^2), H is the ponding depth (m), t is time (day), E is evapotranspiration (m day^{-1}) and P is precipitation (m day^{-1}).

Evaporation from the ponds has been calculated as evapotranspiration using Hargreaves method (equation 7) (Hargreaves & Samani, 1985)

$$\lambda E_{t0} = 0.0023 \times R_A \times TD^{1/2} \times (T + 17.8) \quad (7)$$

Where, λ is Latent heat of vaporization of water (MJ kg^{-1}), E_{t0} is evapotranspiration (mm day^{-1}), R_A is extraterrestrial solar radiation (MJ m^{-2} day^{-1}), TD is the difference between maximum and minimum average monthly temperature (°C**)** and T is mean daily temperature (°C**).**

Linear regression analysis has been used to analyze the sensitivities of (1) natural recharge, (2) Tidal effect of North Sea, (3) Pumping rate and (4) Pond water temperature on infiltration rate. Natural recharge varies seasonally as it is influenced primarily by precipitation and has been hence considered in the study. Tidal effect is suspected to have some impact on the groundwater levels since the site is very close to the North Sea. The shifting of saltwater – freshwater boundary may shift causing variation in daily groundwater levels in the area. Pumping rate is the main driving force in the movement of water in this system and has high potential to influence groundwater

levels and infiltration rates. Temperature of water controls the fluidity of water and might have an impact on the hydraulic conductivity if the media.

In this chapter, we discuss the outcomes of fitting a linear equation to the aforementioned parameters. A good coefficient of determination (R^2) indicates a better sensitivity. This is done using simple linear regression, which attempts to develop a relationship between two variables by fitting a linear equation individually to each observed parameter. Another way of obtaining sensitivities is by performing a multivariate linear regression, where the sensitivities of parameters are assessed in combination. A p-value of 0.05 indicates a 95% probability of the variable to have some effect on the parameter it is being compared to (Abbaspour, 2007). A variable having p-value < 0.05 is considered to be a sensitive parameter.

There is no physical method to measure natural recharge in the area. Hence, it has been calculated by the SCS curve number method (Mockus, 2004). The area adjacent to the pond is a grassland with little vegetation and has dune soil. According to the hydrologic soil group (HSG) classification, the soil in this area represents group A which signifies lower runoff (Mockus, 2004). The curve number for this soil type and land use is 39 (NRCS, 1986). Calculation of natural recharge requires the potential of maximum retention (equation 8) and initial abstraction (equation 9) to obtain the contribution of rainfall to runoff and infiltration.

$$S = \frac{1000}{CN} - 10 \qquad 8$$

Where S is potential of maximum retention after the offset of runoff (in) and CN is curve number (-).

$$I_a = 0.2\,S \qquad 9$$

Where I_a is the initial abstraction (in).

If the rainfall event is greater than initial abstraction, runoff will be experienced. In case the precipitation does not reach the initial abstraction limit, the entire water infiltrates to the ground as natural recharge.

Tidal effects are evaluated by using daily sea level information obtained from sea level station monitoring facility at Oostende, which is 21 km away from the Torreele MAR facility, along the coast of North Sea. Pumping rates and water temperature have been measured on site by the IWVA (Intercommunal Water Company of Veurne-Ambacht), who manages this site.

Viscosity and density are two factors that are directly influenced by temperature. Viscosity of water is calculated using the International Association for the Properties of Water and Steam 1997 (IAPWS 97) (equation 10).

$$\eta(T) = 2.414\, x\, 10^{-5} x\, 10^{\frac{247.8}{T+273.5-140}} \qquad 10$$

Where, $\eta\ (T)$ is the dynamic viscosity (Pa.s) and T is temperature (^{o}C).

Density of water is calculated using equation 11 (Maidment, 1993)

$$\rho(T) = 1000 \times \left(1 - \frac{T+288.9414}{508929.2\times(T+68.12963)} \times (T - 3.9863)^2\right) \qquad 11$$

Where $\rho\ (T)$ is the density (kg m^{-3}).

Kinematic viscosity is calculated as (equation 12) :

$$v = \frac{\eta}{\rho} \qquad 12$$

Where v is kinematic viscosity (m^{2}sec^{-1}).

3.3 Results

Figure 15 is a box plot of the calculated daily infiltration rate through the pond bed per month. It is seen that infiltration rate is the lowest in the winter months and higher in summer, which is in accordance with the problem statement.

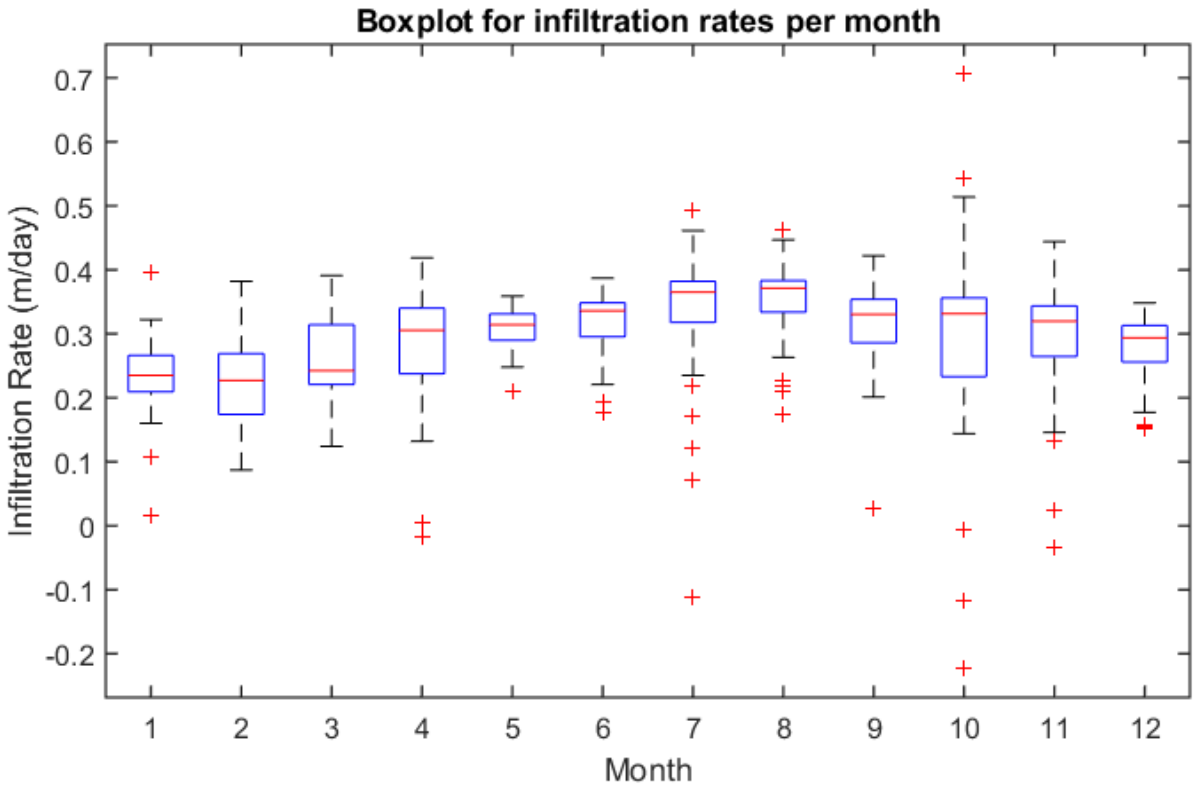

Figure 15. Boxplot for daily infiltration rate for every month starting from January 2015 to December 2016 (1 represents January and 12 represents December)

3.3.1 Simple linear Regression analysis

From the simple linear regression analysis, it is observed that natural recharge and tidal effect of the North Sea do not significantly affect the infiltration rate (figures 16 and 17). However, daily pumping volume and water temperature show a positive correlation (figures 18, 19 and table 2) with infiltration rate. Temperature shows the highest correlation of 0.53 and the maximum slope

of 2.38E-03 with infiltration rate whereas pumping rates have a correlation coefficient of 0.12. From this test, it is inferred that temperature is the most influencing factor in the seasonal variation of infiltration rate through the pond bed.

Table 2. Components of linear relations between the factors and infiltration rates

Factor	***Slope***	***Intercept***	***R^2***
Natural Recharge	-9.60E-04	0.293	0.0001
Daily sea level	6.05E-03	0.204	0.0001
Pumping Rate	2.24E-05	0.119	0.23
Pond water Temperature	2.38E-03	0.288	0.5276

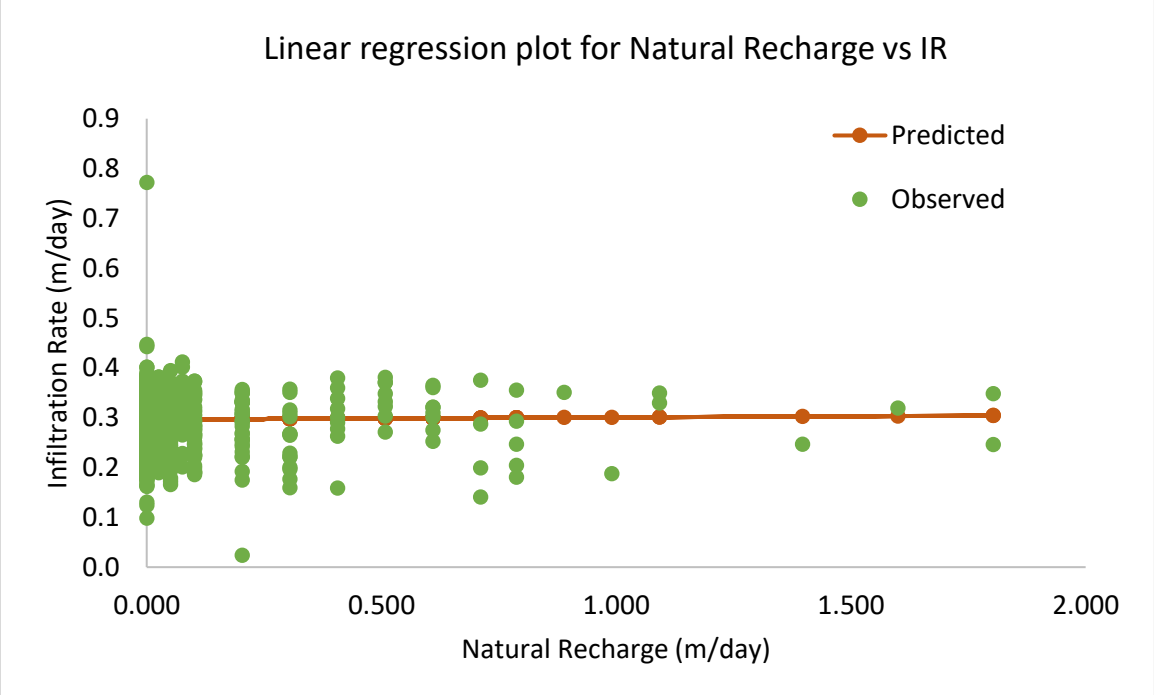

Figure 16. Linear regression plot for natural recharge vs infiltration rate

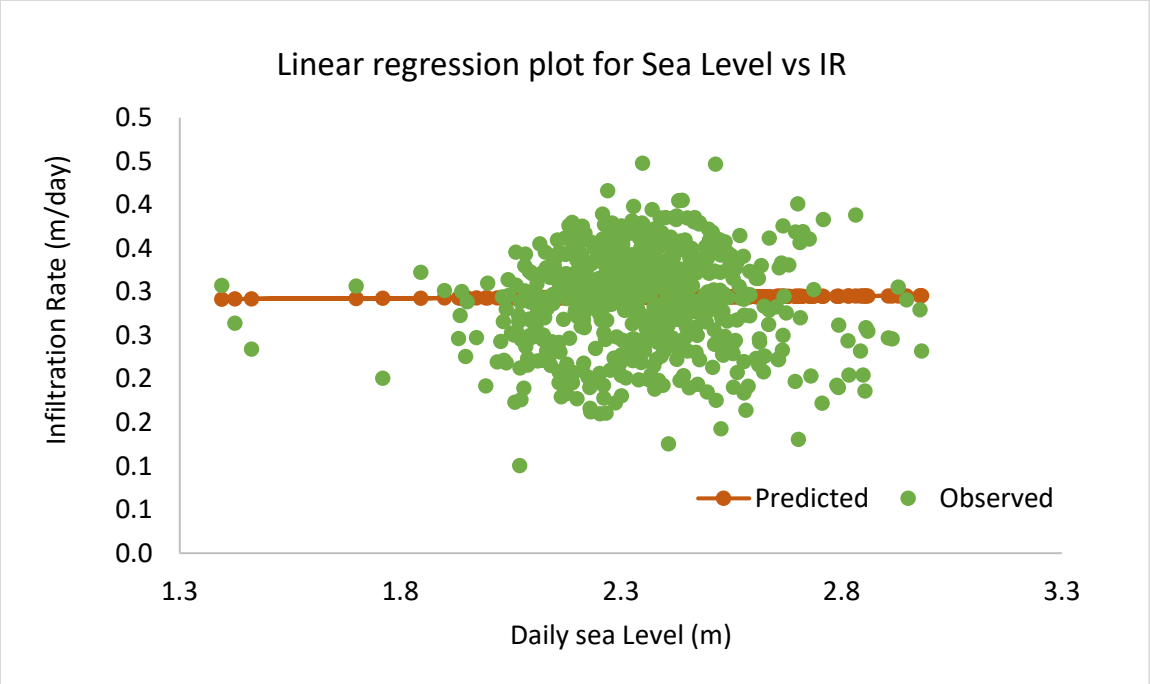

Figure 17. Linear regression plot for daily sea level vs infiltration rate

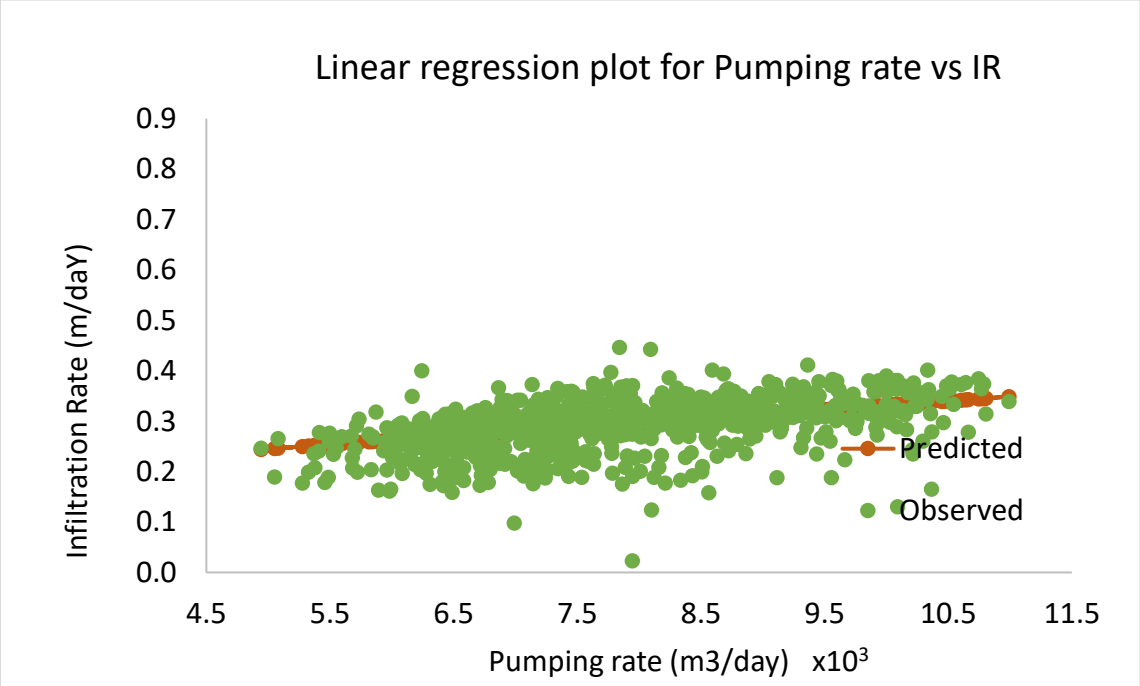

Figure 18. Linear regression plot for daily pumping rate vs infiltration rate

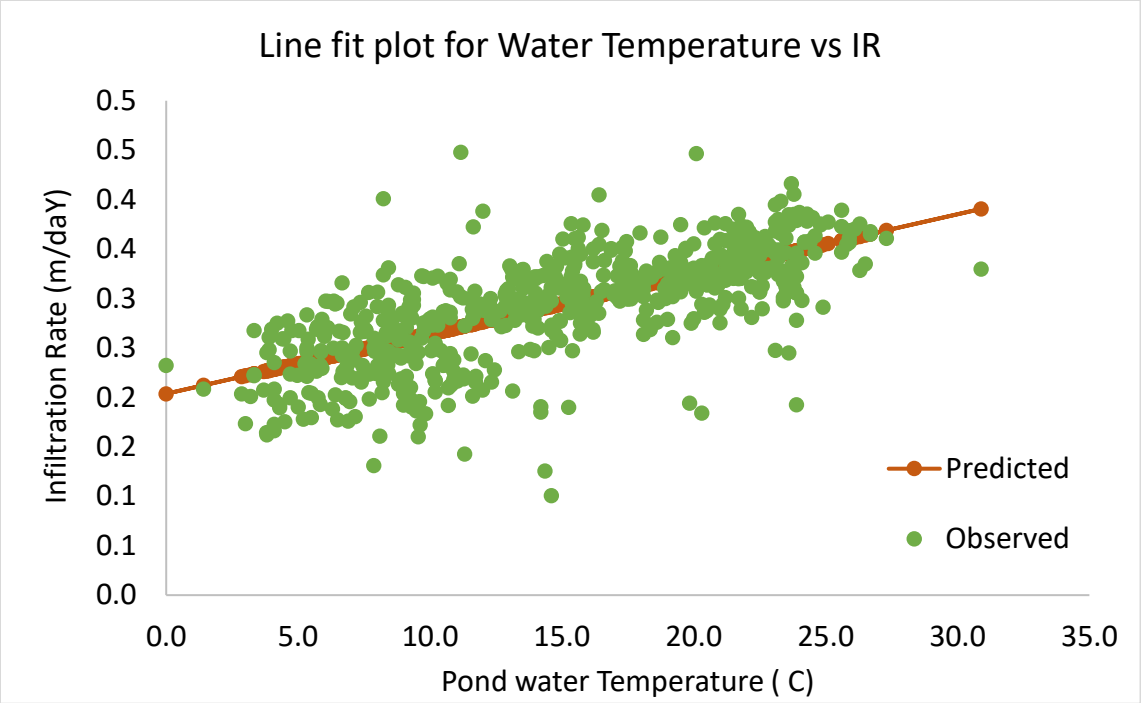

Figure 19. Linear regression plot for mean daily pondwater temperature vs infiltration rate

3.3.2. Multivariate Linear Regression analysis

On performing a multivariate analysis of the 4 factors, the following relation (equation 13) has been obtained:

$$y = 0.167 + 0.011\,x_1 - 0.004x_2 + 3.84 \times 10^{-6}x_3 + 0.005x_4 \qquad 13$$

Where y is predicted infiltration rate, x_1 is natural recharge, x_2 is daily sea level in the North Sea, x_3 is daily pumping rate and x_4 is mean daily pond water temperature.

Equation 13 predicts the infiltration rate with a coefficient of determination of 0.43. Table 3 shows the statistics of the multivariate regression analysis and it is observed that only the pond water temperature (variable x_4) shows the least p-value of 2.39E-59. From figure 20, it can be seen that the observed and predicted infiltration rate shows a fairly good match. However, there are a few outliers in the observed infiltration rates, which may be attributed to human errors involved in

the process of data collection for the parameters in equation 6. Thus, it can be observed from the multivariate regression analysis that pond water temperature is the most dominant factor in controlling the infiltration rate.

Table 3. Components of multivariate linear regression to obtain infiltration rate

	Coefficients	***t Stat***	***P-value***
Intercept	0.1665	7.752553	3.64E-14
Natural Recharge (x_1)	0.011396	1.531668	0.126107
Daily sea level (x_2)	0.003985	0.508899	0.611001
Daily pumping rate (x_3)	3.84E-06	2.560079	0.010697
Pond water Temperature (x_4)	0.005496	18.11734	2.39E-59

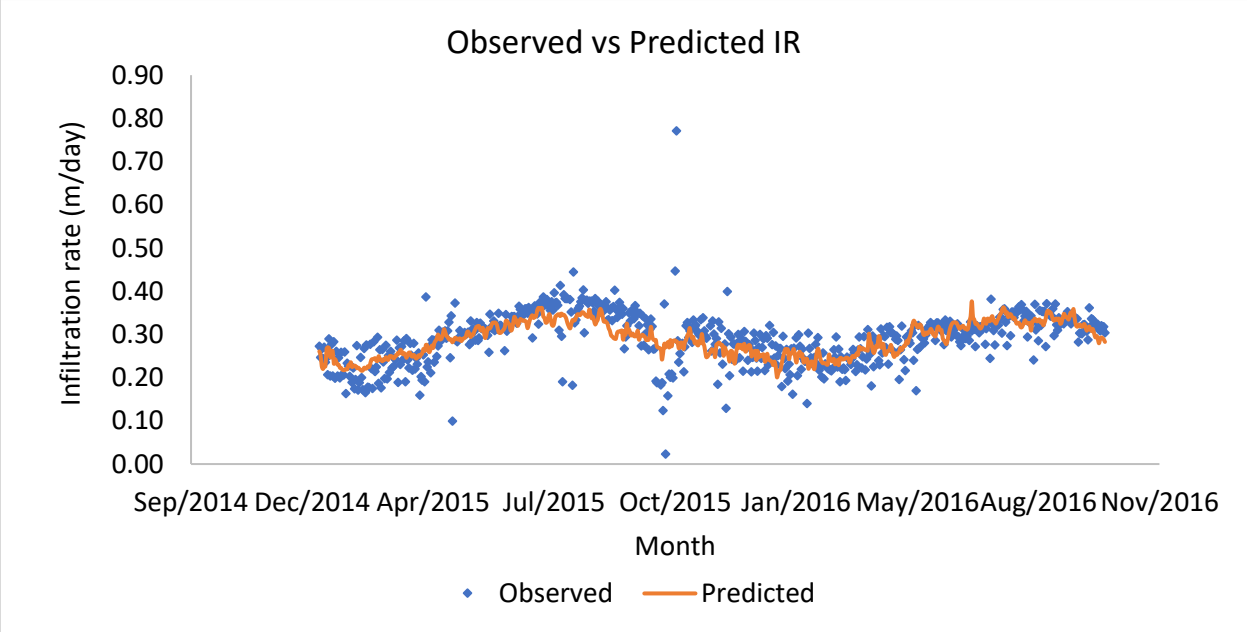

Figure 20. Observed vs Predicted infiltration rate obtained after multivariate regression analysis

3.3.3 Influence of temperature on infiltration rate

As seen in section 3.2.1 and 3.2.2, temperature has the most influence in the variation of infiltration rates across the pond bed. This can also be visually verified from figure 21. Temperature follows a sinusoidal pattern (Vandenbohede & Houtte, 2012) and infiltration rate is also seen to follow a cyclic pattern where the highest rates are observed in summer and lowest in winter. The correlation between temperature and infiltration rate is 0.53.

Viscosity and temperature are the two derivate properties of temperature. Sensitivities of density and viscosity on infiltration rate are checked by using linear regression. It is necessary to know which component of temperature is responsible for temperature to be the dominant factor controlling the variation of infiltration rate. From figures 22 and 23, it is seen that with an increase of both viscosity and density of pond water, the rate of infiltration through pond bed decreases. However, the correlation coefficient between viscosity and infiltration rate is higher than that of density and infiltration rate.

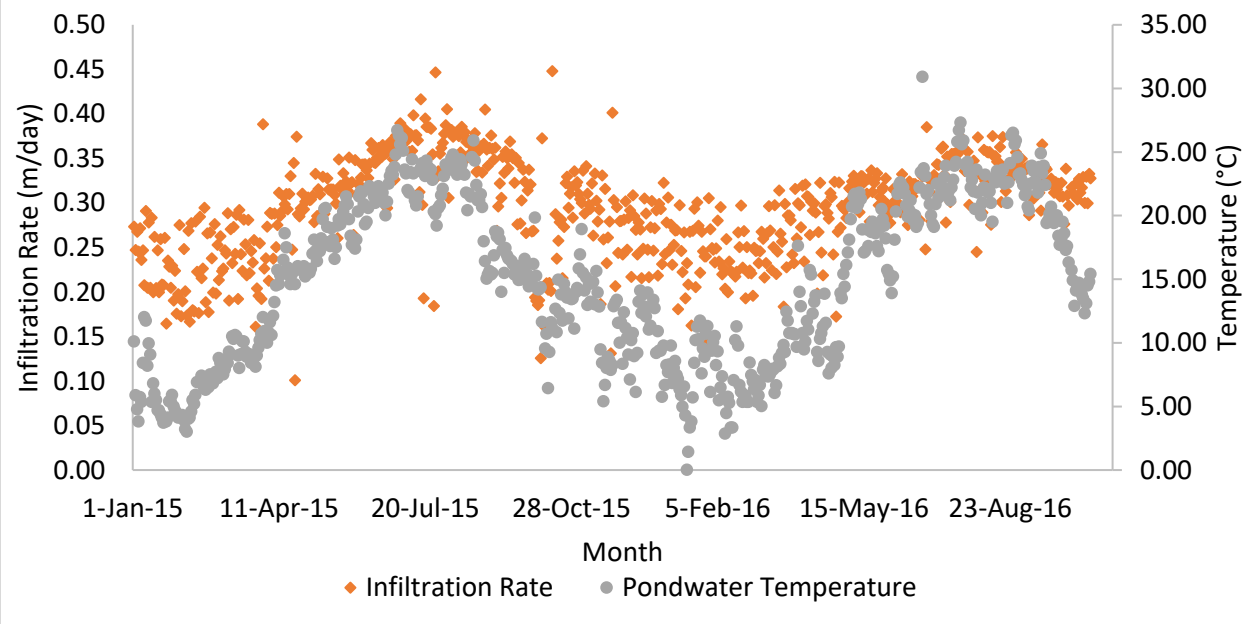

Figure 21. Comparison of mean daily pond water temperature and infiltration rate through pond bed

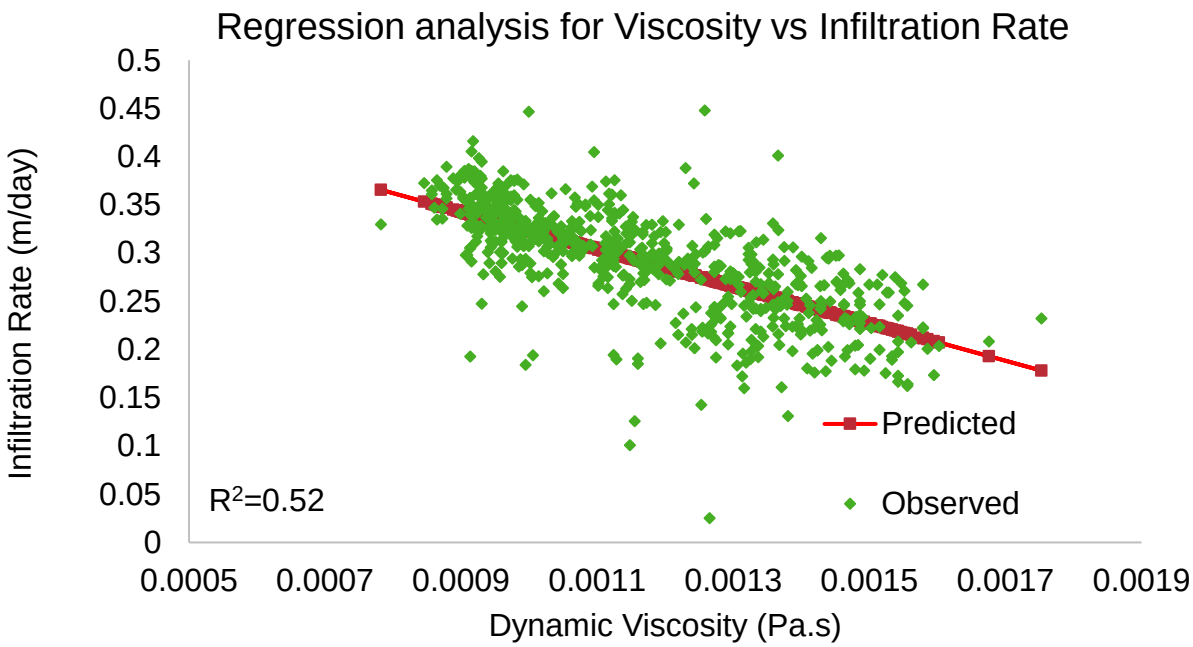

Figure 22. Regression analysis for viscosity of water vs infiltration rate through pond bed

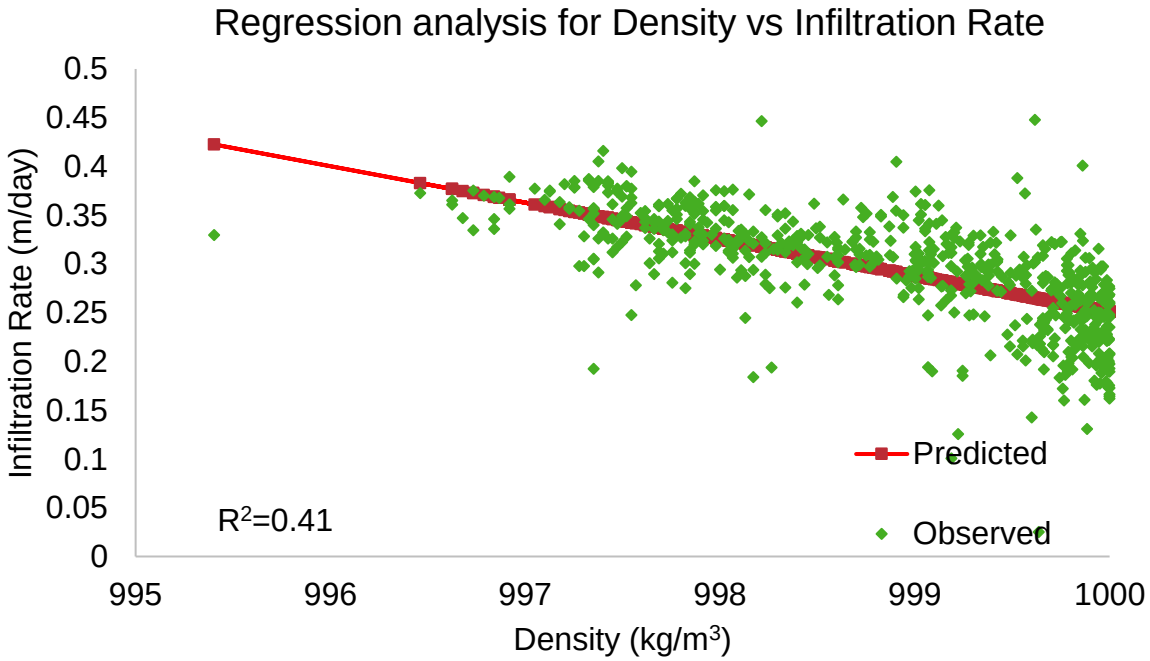

Figure 23. Regression analysis for density of water vs infiltration rate through pond bed

3.4 Discussion

It is to be noted that the rate of change of viscosity per °C change in temperature between 4 to 10 °C is approximately 3 % per °C. Whereas, density changes between the same temperature range is approximately 0.004 % per °C. Hence, the impact of viscosity is higher than that of density.

According to Muskat's relation between hydraulic conductivity and intrinsic permeability (Muskat & Wyckoff, 1937) (equation 14),

$$K = k \times g \times \frac{\rho(T)}{\eta(T)} \quad 14$$

Where K is hydraulic conductivity (m^2sec^{-1}), k is intrinsic permeability (m^2) and g is acceleration due to gravity ($m\ sec^{-2}$). This can also be expressed as (equation 15):

$$K = k \times g \times \frac{1}{\nu(T)}$$

$$\Rightarrow K = k \times g \times f(T) \quad 15$$

Where f is fluidity of water ($sec\ m^{-2}$) which is the inverse of kinematic viscosity (equation 16).

$$f(T) = \frac{1}{\nu(T)} \quad 16$$

Intrinsic permeability is a material dependent property and is assumed to be constant over time in this study. Hence, hydraulic conductivity of soil is directly proportional to the fluidity of water passing through it.

A linear regression analysis shows that the effect of fluidity on infiltration rate is identical to the effect of temperature on IR. The correlation coefficient between fluidity and IR is 0.52 (figure

24). Hence, the variation of density of water has little or no effect on the variation of infiltration rate through the pond bed in the Torreele MAR facility.

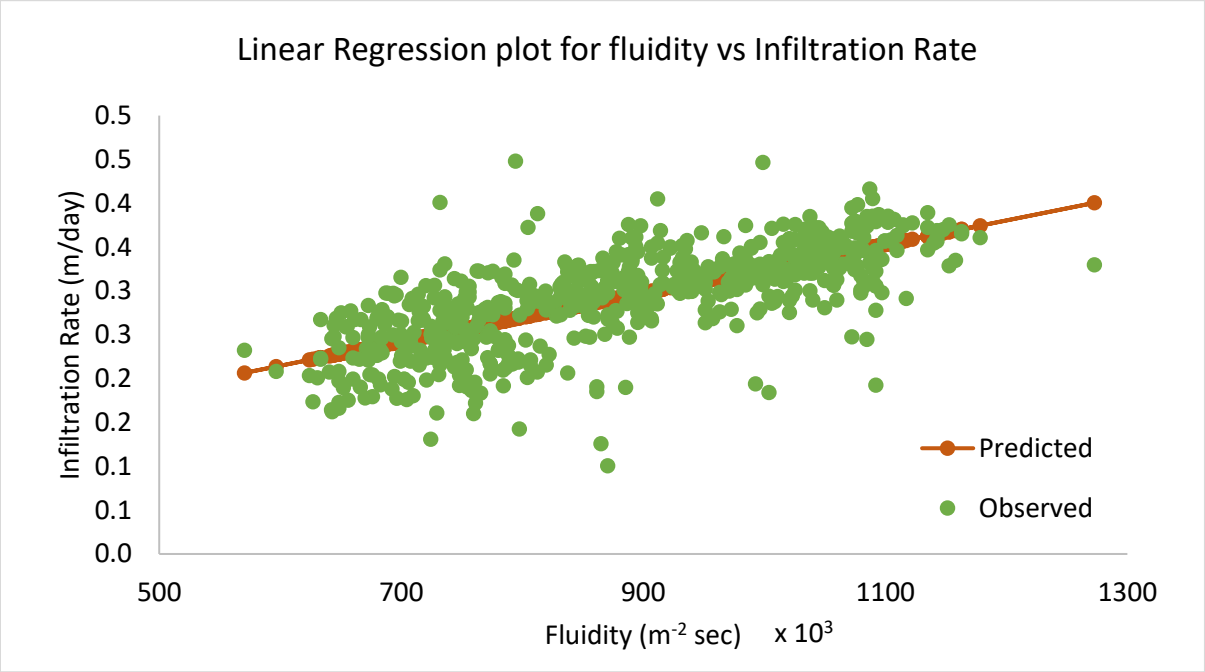

Figure 24. Regression analysis for fluidity of water vs infiltration rate through pond bed

At reference temperature T_{ref}, let the hydraulic conductivity be K_{ref}. According to equation 15,

$$K_{ref} \propto f(T_{ref}) \quad 17$$

Hence, at temperature T, the hydraulic conductivity can be expressed as (equation 18),

$$K(T) = K_{ref} \times \frac{f(T)}{f(T_{ref})} \quad 18$$

The mean temperature of infiltration water is 15 °C. The upper quartile (3rd quartile) of pond water temperature provides the reference for the average hydraulic conductivities in summer and the lower quartile (1st quartile) provides reference for the winter conductivities. The upper quartile of pond water temperature is at 9.3 °C and the lower quartile is at 21 °C (figure 25).

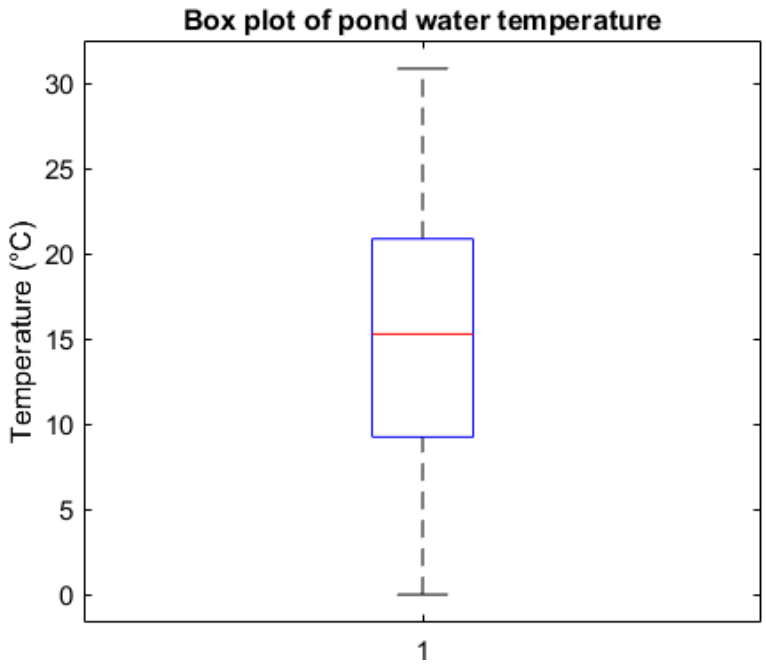

Figure 25. Box plot of pond water temperature

After fitting these values to equation 18, it is observed that the hydraulic conductivity increases by 15 % in summer and decreases by 14.7 % in winter. In other words, there is a 30% increase in hydraulic conductivity of the pond bed in summer as compared to winter. The change in hydraulic conductivity is not constant through the entire soil profile since the temperature variation with depth is not uniform. According to (Vandenbohede & Houtte, 2012), the temperature of water changes as it moves down, which is influenced by the existing groundwater residing in the aquifer. Temperature becomes constant after a depth of 25 m below the ground.

CHAPTER IV

GROUNDWATER FLOW MODEL OF TORREELE MAR FACILITY

4.1 Visual MODFLOW

Visual MODFLOW is a 3-dimensional groundwater flow and contaminant transport model package that uses flow engines such as MODFLOW-96, MODFLOW-2000, MODFLOW-2005, MODFLOW-SURFACT, SEAWAT, MODFLOW-NWT and transport engines such as MT3D, MT3DMS, RT3D, and PHT3D. Particle tracking is also a part of this software package and is done by MODPATH. The primary governing equations for groundwater flow are Darcy Law (equation 19) and 3D flow equation (equation 20).

$$q_x = -K_x \frac{dh}{dx} \tag{19}$$

Where, q_x is the specific discharge or Darcy velocity, K_x is hydraulic conductivity in x-direction and $\frac{dh}{dx}$ is the hydraulic gradient.

$$\frac{\partial}{\partial x}\left(K_x \frac{\partial h}{\partial x}\right) + \frac{\partial}{\partial y}\left(K_y \frac{\partial h}{\partial y}\right) + \frac{\partial}{\partial z}\left(K_z \frac{\partial h}{\partial z}\right) = S_s \frac{\partial h}{\partial t} \tag{20}$$

Where K_x, K_y and K_z are the hydraulic conductivities and $\frac{dh}{dx}$, $\frac{dh}{dy}$ and $\frac{dh}{dz}$ are the hydraulic gradients in x, y and z directions respectively. S_s is specific storage and $\frac{\partial h}{\partial t}$ is the change in hydraulic head over time. Equation 20 is a 3D second order partial differential equation that is numerically solved by MODFLOW.

4.2 Description of conceptual models

Visual MODFLOW has been used in this study to develop a groundwater flow model representing the area close to the infiltration ponds for the time period of January 2015 to March 2016 verify the variation of infiltration rates. Two models have been developed to represent the

conditions for summer and winter seasons. Constant pumping and infiltration rates have been used in each model to observe the impact of leakance through pond bed. From section 3.3, it is seen that there is a 30% rise in hydraulic conductivity of the pond bed. The objective of this chapter is to observe the heads at the location of the monitoring wells and verify how closely the simulated heads under known circumstances match the observed heads.

This section deals with the boundary conditions, water budget and hydraulic parameters used in the model. The model area is 1100 m long, 630 m wide and is centered on the infiltration ponds. The model has been slightly rotated to match the north boundary to the coast of North Sea (figure 26.a). It is divided into 110 columns and 63 rows each cell having a 1 m x 1 m area. The aquifer thickness is 31 m and is divided into 32 layers of 1 m depth except for between 3 and 4 mTAW where the layers are of 0.5 m depth (figure 26.b). The sources of water in this model are recharge through the pond beds and natural recharge in the area. There are 137 extraction wells surrounding the ponds, which act as the sinks (figure 27).

The hydraulic conductivity and specific yield of the layers have been set based on borehole measurements obtained at the location of WP6 and from the parameters used in previously developed models for the area (Vandenbohede & Houtte, 2012). The borehole record and the translation of soil types present in the area are made in accordance to the USDA soil textures. The borehole log is provided in Appendix B (figure 33) and the translation is provided in Appendix C (table 6). From section 3.4, it is seen that there is a sharp vertical gradient at the location of WP_21 and WP_23. A low permeable zone is introduced in the model just under the bed of both ponds to match the effect of vertical gradient. Figure 28 shows a two-dimensional vertical cross-section of the model with the various hydraulic conductivity zones used. Table 4 represent the conductivity values for the zones. Boundary conditions have been set based on groundwater flow models

developed previously for Torreele MAR facility (Vandenbohede & Houtte, 2012) and in reference to section 3.2.1.

MODFLOW Lake package (LAK3) has been used to model the infiltration ponds in both the models. The lake bottom is at 6.24 mTAW. The average precipitation is 345 mm/year and the evaporation is 450 mm/year in both the models. Heads have been simulated at monitoring wells WP 6.2, WP 22.2 and WP 42.2. Both the models have been calibrated to match the heads in the aforementioned monitoring wells.

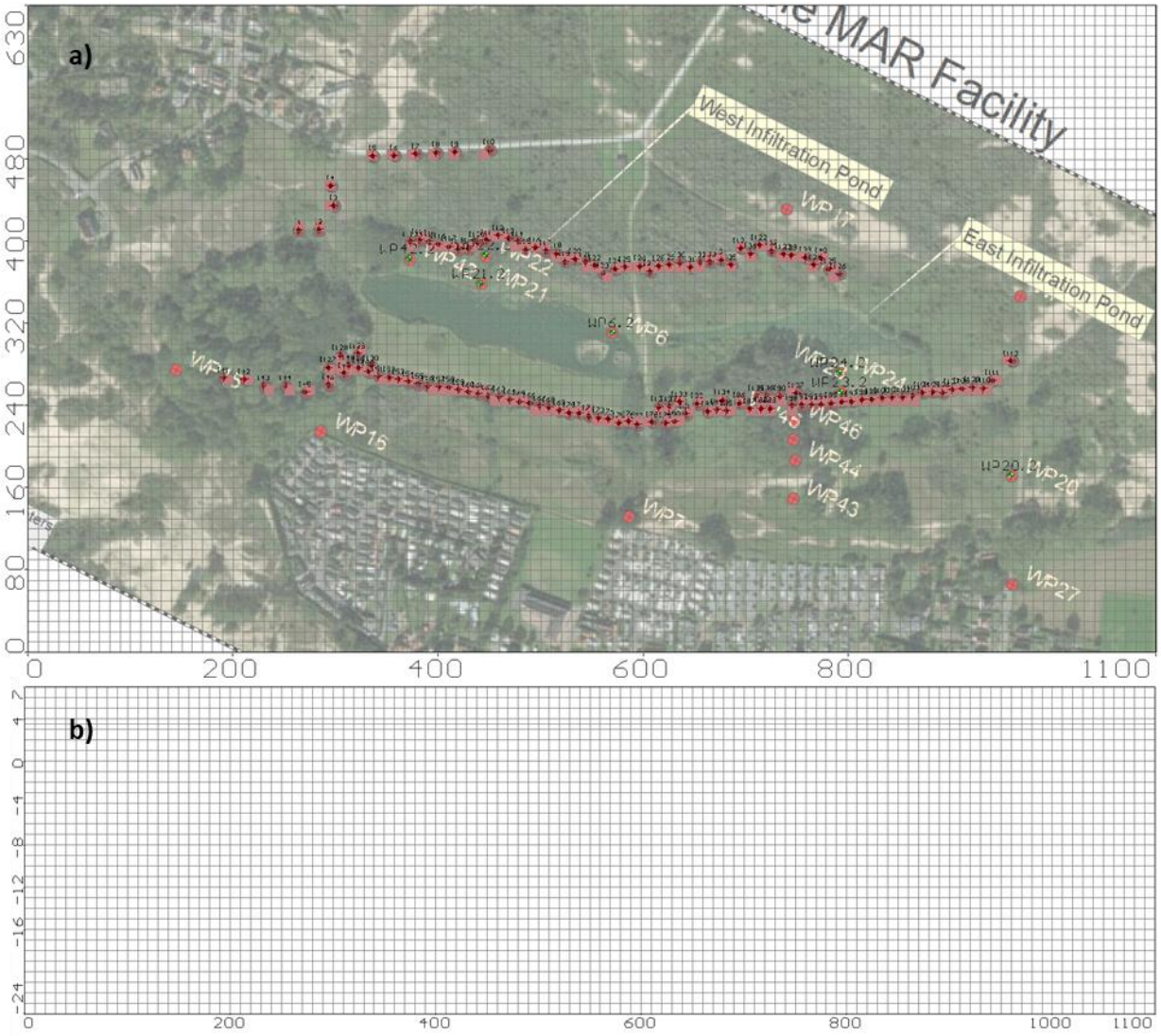

Figure 26. Layout of Torreele MAR MODFLOW model. a) Top view and b) Front view

The statistical indices used to assess the goodness of fit of the models are coefficient of determination (R^2) and Root Mean Square Error (RMSE). RMSE is the measure of the standard deviation of the errors between observed and predicted values. It is expressed as (equation 21),

$$RMSE = \sqrt{\frac{\sum_{i=1}^{n}(Y_i{}^{obs} - Y_i{}^{sim})^2}{n}} \qquad 21$$

Where $Y_i{}^{obs}$ is the i[th]-observed value and $Y_i{}^{sim}$ is the i[th]-simulated value and n is the number of terms.

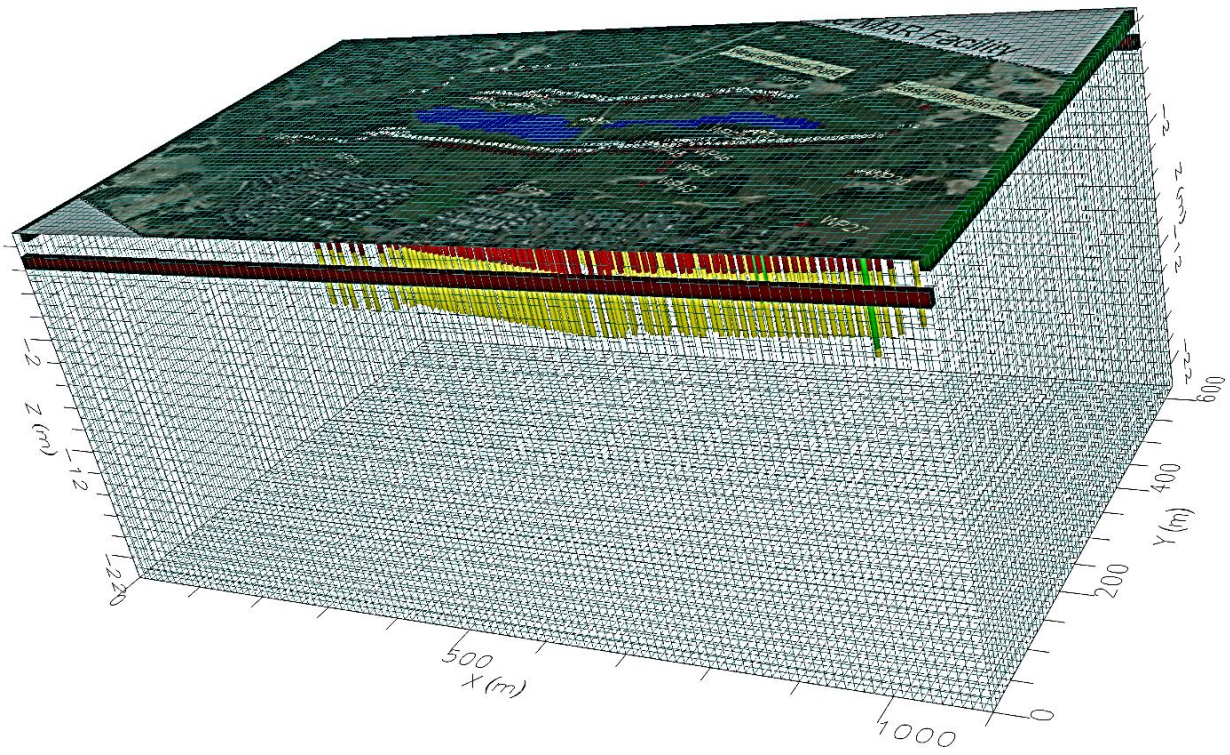

Figure 27. 3D view of Pumping wells and boundary conditions

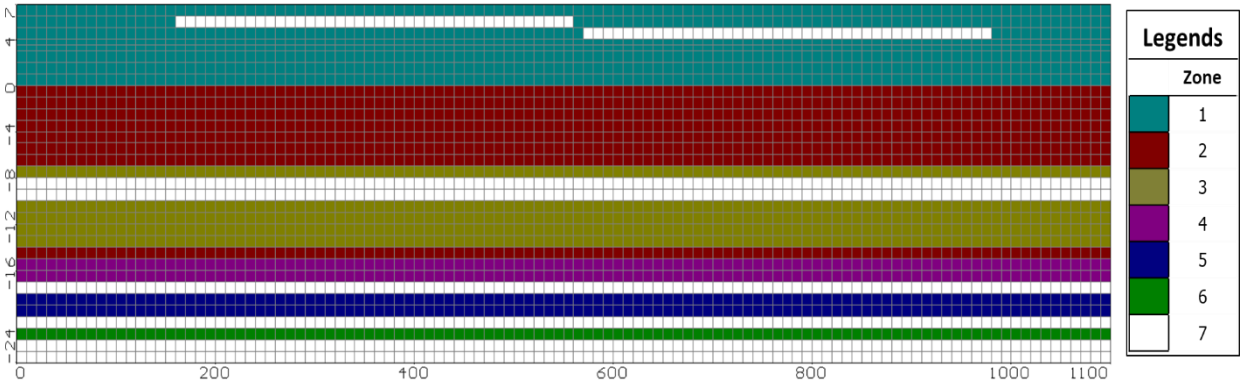

Figure 28. Zones of hydraulic conductivity in the model

Table 4. Conductivity zones used in the models

Zone	K_x	K_y	K_z
1	20	20	1.00
2	15	15	0.75
3	5	5	0.25
4	50	50	2.5
5	25	25	2.5
6	0.5	0.5	0.05
7	2.5	2.5	0.125

4.2.1 Groundwater flow model representing summer conditions

The first MODFLOW model developed for the summer months (June-July-August) using conditions from summer (JJA) of 2015 uses a North-South constant head boundary of 3.5 mTAW based on the analysis of heads in section 3.2.1. The East-West boundary is defined as a general head boundary in reference to the mean lake stage during this period. A constant pumping rate of 8400 m^3day^{-1} and an inflow rate of 6080 m^3day^{-1} has been used for this model, which represents the mean pumping rate and inflow rate during this period. The mean lake stage is 6.9 mTAW.

Leakance through pond bed is set as 0.39 day^{-1}, which is 30 % higher than the leakance of pond bed in winter.

4.2.2 Groundwater flow model representing winter conditions

A second MODFLOW model has been developed for the winter months (December-January-February) using conditions from winter (DJF) of 2015-2016. It uses a constant head North-South boundary of 4 mTAW and the East-West boundary is a general head boundary which follows the mean lake stage during this period. The pumping rate is set at 7000 m^3day^{-1} and the inflow rate to the lake is 4310 m^3day^{-1}. The mean lake stage is 6.97 mTAW and pond bed leakance is 0.30 day^{-1}.

4.3 Results

WP 6, WP 22 and WP 42 are the monitoring wells located within the pumping well barrier and have been used to observe the impact of variation infiltration rates for summer and winter. Figures 29.a and 29.b show the comparison between simulated heads with summer conditions, heads with winter conditions and observed heads. A satisfactory fit is obtained between the observed and simulated heads in summer months for the summer model as well as in the winter months for the winter model in all the wells (table 5).

a) Summer Model Results

b) Winter Model Results

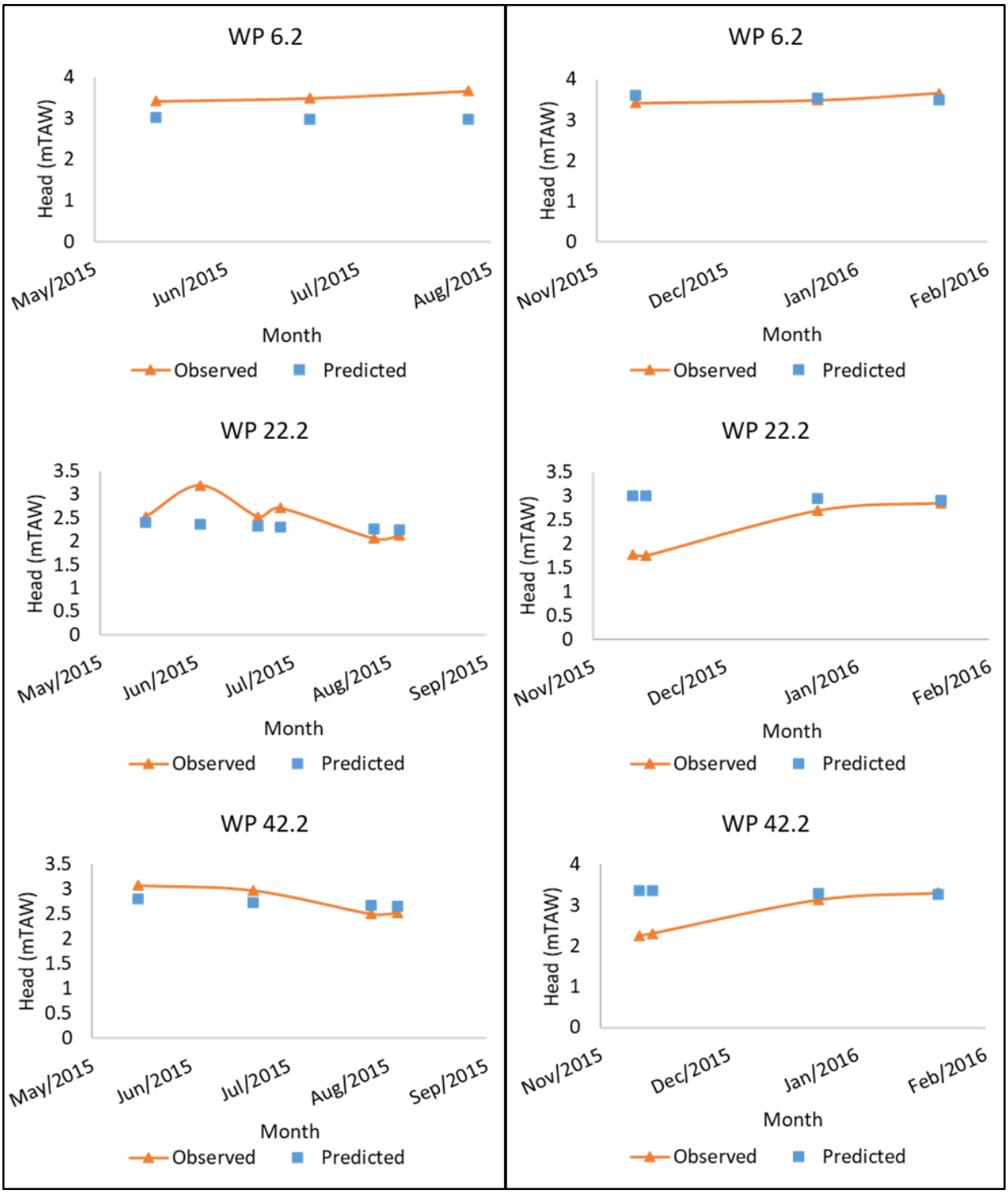

Figure 29. Observed vs simulated heads from MODFLOW model at Torreele MAR facility. a) Results from summer model during summer months (JJA); b) Results from winter model for winter months (DJF)

Table 5. Statistical indices showing goodness of fit of the two groundwater flow models at different monitoring wells

Period	Monitoring wells	RMSE (m)		R^2	
		Summer Model	Winter Model	Summer Model	Winter Model
Summer 2015	WP 6.2	0.18	-	0.68	-
	WP 22.2	0.21	-	0.86	-
	WP 42.2	0.50	-	0.44	-
Winter 2015-2016	WP 6.2	-	0.15	-	0.88
	WP 22.2	-	0.90	-	0.94
	WP 42.2	-	0.77	-	0.95

Figure 30 shows the horizontal cross-section through the unconfined aquifer at the location of WP 6 parallel to the East-West Boundary (column 58) and figure 31 shows the same at the location of WP 42 (column 38). For both the cross-sections, summer and winter models have been used to describe the respective time. Figures 30.a and 31.a show the scenario from the summer model on 07/14/2015 and figures 30.b and 31.b show the scenario from the winter model on 01/12/2016. The arrows represent the direction and magnitude of the groundwater flow rates. The most dominant flow under the ponds are the vertical flow. The maximum Darcy velocity through the recharge ponds in winter is 0.22 m day^{-1} whereas in summer the maximum Darcy velocity is 0.31 m day^{-1}.

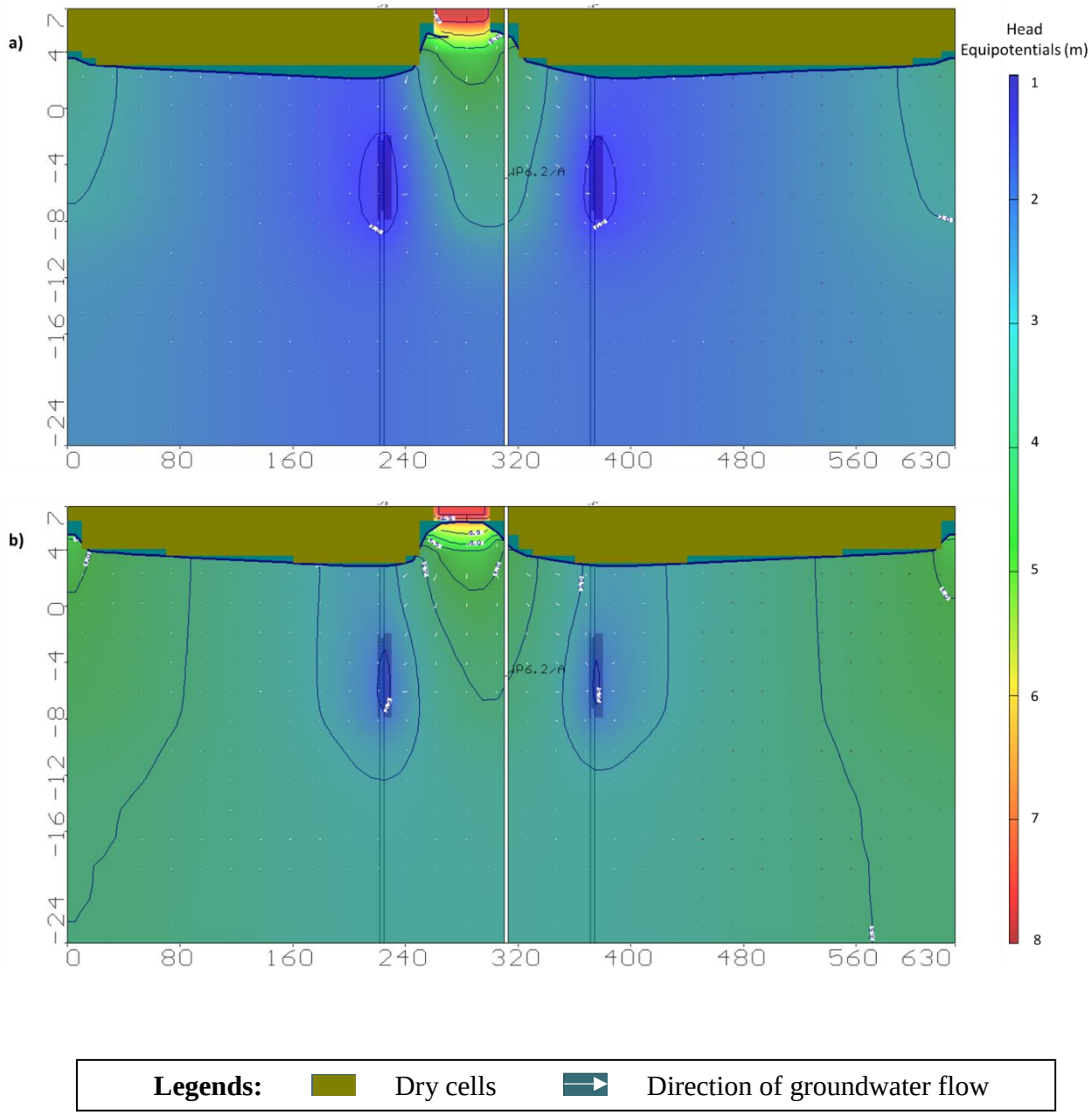

Figure 30. Horizontal cross-section of the aquifer at the location of WP 6.2 a) on 7/14/2015 from the summer groundwater flow model and b) on 1/12/2016 from winter groundwater flow model

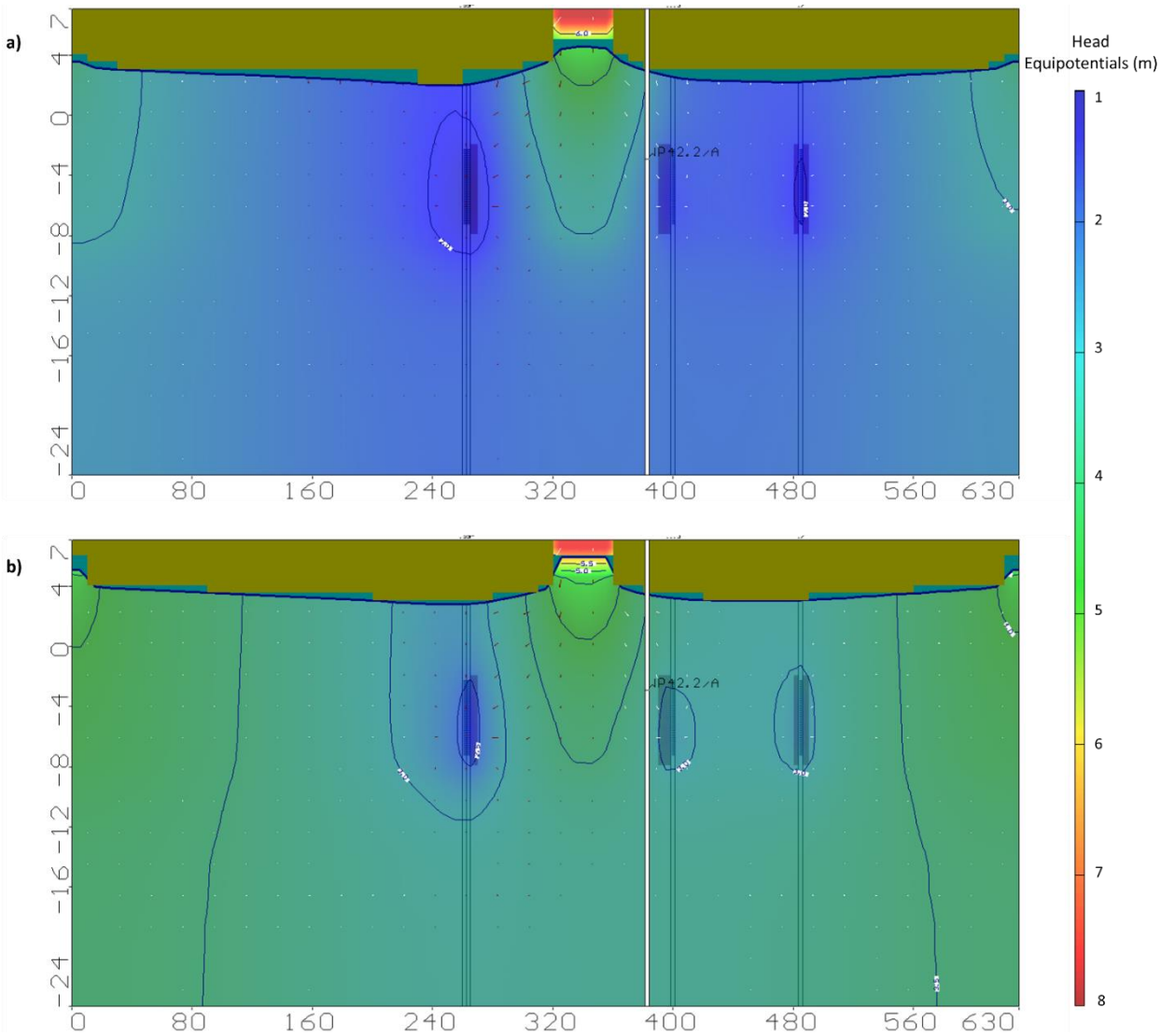

Figure 31. Horizontal cross-section of the aquifer at the location of WP 42.2 a) on 7/14/2015 from the summer groundwater flow model and b) on 1/12/2016 from winter groundwater flow model

Legends:	Dry cells	Direction of groundwater flow

4.4 Discussion

The models have been developed with constant pumping and infiltration rates to match the respective seasons. The target of the 2 models is to depict the impact of leakance on the recharge rate and the flow velocity. Pond bed leakance is expressed as (equation 22),

$$L = \frac{K_z}{b} \quad 22$$

Where, L is leakance (day $^{-1}$), K_z is vertical hydraulic conductivity and b is the thickness of pond bed.

This can also be written as (equation 23),

$$L \propto K_z \quad 23$$

From section 4.3, it is seen that the there is a 30% rise in hydraulic conductivity of the pond bed during the summer months as compared to the winter months. Similarly, the summer model uses a leakance value that is 30% higher than the leakance value of winter. The results obtained from the two models at the respective time zones show a good match. The combined RMSE is 0.74 for WP 22.2, 0.66 m for WP 42.2 and 0.39 for WP 6.2. The variation in accuracy is caused due to the spatial variation of hydraulic parameters in soil. WP 42.2 and WP 22.2 show a higher RMSE as the model assumes a single value for the hydraulic parameters for a single layer. However, WP 6.2 shows a fairly good match as it is located very close to the ponds and it reflects the vertical flux well. This can be visually verified by figure 30 and 31, which show the magnitude and direction of groundwater flow at the location of WP 6.2 and WP 42.2 respectively for the summer and winter models.

The residence time of water is responsible for the high RMSE in the models. The response of the heads in WP 6.2 to the change in temperature conditions is faster than the other two. The

heads in WP 6.2 in December fairly relates to the simulated heads in the winter model. However, in WP 22.2 and WP 42.2 the heads in December are very low and they correspond to the heads in summer scenario. This may be attributed to the distance travelled by the water before it reaches the pumping wells. The variation in residence time occurs due to the presence of a low permeable soil layer on the north side of the west pond. The overall deviation in observed and simulated heads from the models are due to the fact that hydraulic conductivity is constantly varying with time as temperature changes. However, in the models, the conductivity values have been kept constant all throughout each season.

It is observed from the hypothetical scenarios that the maximum Darcy velocity through the pond bed during summer is 0.31 m day^{-1} and that during the winter is 0.22 m day^{-1}. This velocity can also be accounted as the seepage rate or recharge rate. The reduction in winter recharge rate is hence reduced by about 27 %. This suggests that the variation in observed heads is partly influenced by leakance, which is proportional to the vertical hydraulic conductivity of the pond bed.

CHAPTER V

CONCLUSION AND FUTURE WORK

The overall objective of this was to identify the primary factor responsible for the seasonal variation of recharge rate from the infiltration ponds at the Torreele MAR facility in Belgium. Infiltration rates across the pond bed have been studied for a period of 2 years and lower infiltration rates have been noticed in the winter months. The infiltration capacity is approximately 50 to 100 % higher in summer as compared to that in winter. Two major factors impacting this variation are variation in hydraulic gradient and hydraulic conductivity.

Observed heads at the monitoring wells are mostly found to be higher in winters and lower in summers, creating a higher gradient in summers. 32 % reduction in vertical hydraulic gradient have been observed in the top portion of the aquifer which directly influences the recharge rates. Regarding the variation of hydraulic conductivity, temperature has been identified as the dominant factor influencing this process. Results show that there is a strong correlation between temperature and infiltration rate on a daily scale. The temporal variation of temperature causes variation in kinematic viscosity, which plays an important role in the flow of water. With increase in viscosity of recharge water, higher resistance is imparted by the pond bed to the flow of water.

In addition, the temperature of water influences the hydraulic conductivity of the soil. With the data obtained from the Torreele MAR site, it is theoretically found that there is a 30 % increase in conductivity in summer as compared to winter. Lowering of temperature causes a reduction in hydraulic conductivity, thereby providing additional resistance to the flow of water through the pond bed. MODFLOW models have been used to simulate different conditions for summer and

winter and it is found that with a lower leakance of the pond bed in the winter months, the recharge rate decreases by about 27 %. Combining the effects of both gradient and conductivity variation, it was found that the recharge rate in winter months reduced by about 72 % as compared to that in summer, which was consistent with the findings of Vandenbohede & Houtte (2012).

Temperature of recharge water changes as it moves into the subsurface and it is highly influenced by the previously residing water. Temperature at different depths in the aquifer creates a definite response in the conductivity of the media. Lack of temperature data at multiple depths hindered the study of the impact of groundwater temperature on the soil properties. This can be a scope of future study and would greatly enhance the understanding of the flux in the area.

REFERENCES

Abbaspour, K. C. (2007). User Manual for SWAT-CUP, SWAT Calibration and Uncertainty Analysis Programs. *Swiss Federal Institute of Aquatic Science and Technology, Eawag, Duebendorf, Switzerland*.

Constantz, J. (1998). Interaction between stream temperature, streamflow, and groundwater exchanges in alpine streams. *Water Resources Research*, *34*(7), 1609–1615. https://doi.org/10.1029/98WR00998

Constantz, J., & Murphy, F. (1991). The temperature dependence of ponded infiltration under isothermal conditions. *Journal of Hydrology*, *122*(1–4), 119–128.

George H. Hargreaves, & Zohrab A. Samani. (1985). Reference Crop Evapotranspiration from Temperature. *Applied Engineering in Agriculture*, *1*(2), 96–99. https://doi.org/10.13031/2013.26773

Koza, J. R. (1994). Genetic programming as a means for programming computers by natural selection. *Statistics and Computing*, *4*(2), 87–112. https://doi.org/10.1007/BF00175355

Lin, C., Greenwald, D., & Banin, A. (2003). Temperature dependence of infiltration rate during large scale water recharge into soils. *Soil Sci. Soc. Am. J.*, *67*(2), 487–493. https://doi.org/10.2136/sssaj2003.4870

Loizeau, S., Rossier, Y., Gaudet, J., Refloch, A., Besnard, K., Angulo-jaramillo, R., et al. (2017). Water infiltration in an aquifer recharge basin affected by temperature and air entrapment, *65*(3), 222–233. https://doi.org/10.1515/johh-2017-0010

Maidment, D. R. (1993). *Handbook of Hydrology*. *New York* (Vol. no. 28). McGraw-Hill New York. https://doi.org/10.1016/0141-4607(86)90100-9

Mockus, V. (2004). *National Engineering Handbook: Part 630—Hydrology*. *USDA Soil Conservation Service: Washington, DC, USA*.

Moriasi, D. N., Arnold, J. G., Van Liew, M. W., Binger, R. L., Harmel, R. D., & Veith, T. L. (2007). Model evaluation guidelines for systematic quantification of accuracy in watershed simulations. *Transactions of the ASABE*, *50*(3), 885–900. https://doi.org/10.13031/2013.23153

Muskat, M., & Wyckoff, R. D. (1937). Flow of homogeneous fluids through porous media.

NRCS. (1986). *Urban Hydrology for Small Watersheds TR-55*. *USDA Natural Resource Conservation Service Conservation Engeneering Division Technical Release 55*. US Dept. of Agriculture, Soil Conservation Service, Engineering Division. https://doi.org/Technical Release 55

NRMMC, E. (2008). AHMC, Australian guidelines for water recycling: Managing health and environmental risks (Phase 2): Augmentation of drinking water supplies, Environment Protection and Heritage Council, National Health and Medical Research Council. *Natural Resource Management Ministerial Council, Canberra*.

Pantoula, V. A. (2012). *Numerical simulation of alternatives for optimizing infiltration of tertiary treated wastewater in the dune aquifer of St-André, Koksijde, Belgium* (Vol. 1).

Sheng, Z. (2005). An aquifer storage and recovery system with reclaimed wastewater to preserve native groundwater resources in El Paso, Texas. *Journal of Environmental Management*, *75*(4 SPEC. ISS.), 367–377. https://doi.org/10.1016/j.jenvman.2004.10.007

Sheng, Z., & Zhao, X. (2015). Special Issue on Managed Aquifer Recharge: Powerful Management Tool for Meeting Water Resources Challenges. *Journal of Hydrologic Engineering*, *20*(3), B2014001. https://doi.org/10.1061/(ASCE)HE.1943-5584.0001139

Todd, D. K. (1974). Salt-Water Intrusion and Its Control Author (s): David K . Todd Reviewed work (s): Source : Journal (American Water Works Association), Vol . 66 , No . 3 , Ground Water (March Published by : American Water Works Association Stable URL : http://www., *66*(3), 180–187.

Van Houtte, E., & Verbauwhede, J. (2012). Sustainable groundwater management using reclaimed water: The Torreele/St-André case in Flanders, Belgium. *Journal of Water Supply: Research and Technology - AQUA*, *61*(8), 473–483. https://doi.org/10.2166/aqua.2012.057

Vandenbohede, A., & Houtte, E. Van. (2012). Heat transport and temperature distribution during managed artificial recharge with surface ponds. *Journal of Hydrology*, *472–473*, 77–89. https://doi.org/10.1016/j.jhydrol.2012.09.028

Vandenbohede, A., & Lebbe, L. (2012). Groundwater chemistry patterns in the phreatic aquifer of the central Belgian coastal plain. *Applied Geochemistry*, *27*(1), 22–36. https://doi.org/10.1016/j.apgeochem.2011.08.012

Vandenbohede, A., Van Houtte, E., & Lebbe, L. (2008a). Groundwater flow in the vicinity of two artificial recharge ponds in the Belgian coastal dunes. *Hydrogeology Journal*, *16*(8), 1669–1681. https://doi.org/10.1007/s10040-008-0326-x

Vandenbohede, A., Van Houtte, E., & Lebbe, L. (2008b). Sustainable groundwater extraction in coastal areas: A Belgian example. *Environmental Geology*, *57*(4), 735–747. https://doi.org/10.1007/s00254-008-1351-8

APPENDIX A

GENETIC PROGRAMMING EQUATION

The equation obtained by Genetic Programming to compute temperature of pond water is expressed as (equation 24),

Y=times(sin(plus(X1,plus(plus(max(X2,X2),abs(X2)),cos(times(times(abs(minus(plus(times(abs(minus(plus(X1,plus(max(plus(min(X1,X2),X2),abs(X2)),min(times(minus(X2,X2),X1),plus(X1,min(minus(X2,abs(min(cos(plus(X2,mylog(X2))),times(cos(X2),X2)))),plus(X1,X1)))))),mylog(times(sin(minus(mylog(minus(mylog(X2),X2)),X2)),X1)))),cos(sin(sin(abs(X2))))),cos(X1)),mylog(times(sin(minus(plus(max(X2,mylog(X2)),abs(X2)),X2)),cos(X2))))),cos(mylog(abs(minus(mylog(minus(X1,X2)),times(sin(X1),X2)))))),X1))))),X1) 24

Where, Y is the pond water temperature, X1 is minimum air temperature and X2 is maximum air temperature.

The equation tree is given in figure 32.

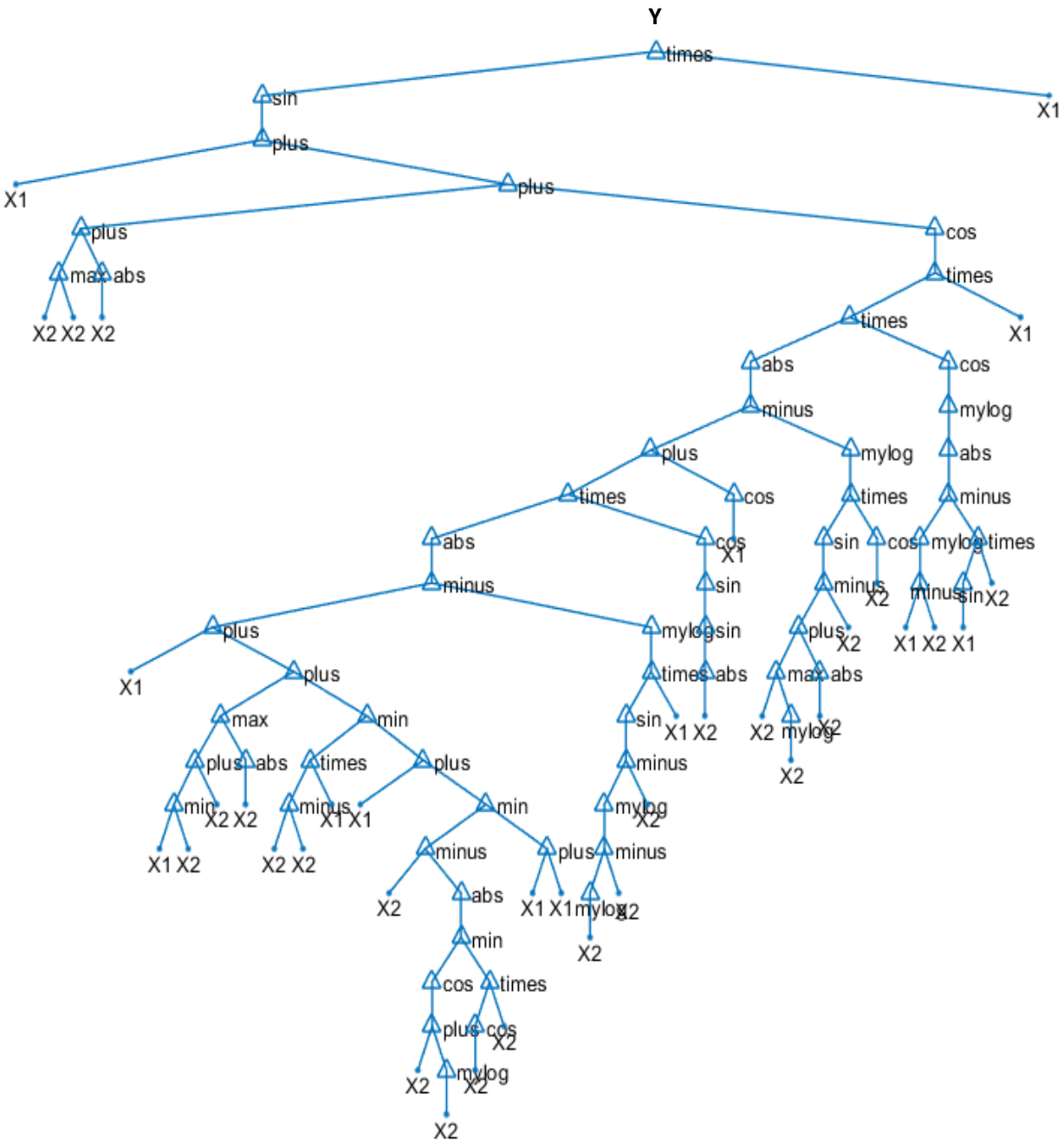

Figure 32. Genetic Programming equation tree for prediction of pond water temperature where X1 is the minimum air temperature, X2 is the maximum air temperature and Y is pond water temperature

APPENDIX B

BOREHOLE LOG AT WP 6

Vlaanderen
is ondergrond

DOV Boorrapport

Boring

Proefnummer:	B/3-85040	Aanvangsdatum:	25/10/1993
X (mLambert):	29964.2 (XY_methode onbekend)	Uitvoeringsmethode:	spoelboring
Y (mLambert):	201827.7 (XY_methode onbekend)	Diepte (m):	0.00 - 32.20
Z (mTAW):	6.68 (Z_methode onbekend)	Water op (m):	
Gemeente:	Koksijde (Koksijde)		
Uitvoerder:	Intercommunale Waterleidingsmaatschappij van Veurne-Ambacht (IWVA)		

Lithologische beschrijving - 25/10/1993

Auteur(s): Van Houtte, E. (Universiteit Gent (UGent)) Betrouwbaarheid: goed

Van(m)	Tot(m)	M	Beschrijving
0.00	0.50		geel fijn zand met roestbrokken
0.50	1.00		geel schelphoudend fijn zand
1.00	2.00		geel weinig schelphoudend fijn zand
2.00	2.20		geel weinig schelphoudend fijn zand, maar weinig veenhoudend
2.20	3.00		geel weinig schelphoudend fijn zand
3.00	4.50		geel weinig schelphoudend fijn zand, maar met weinig leembrokjes
4.50	5.50		geel weinig schelphoudend fijn zand met zeer weinig leembrokjes en roestfragmenten
5.50	6.20		grijsbruin weinig schelphoudend fijn zand
6.20	7.50		donkergrijs weinig schelphoudend fijn zand
7.50	10.00		grijs schelphoudend middelmatig zand met brokken zwarte veenhoudende leem
10.00	11.50		grijs schelphoudend middelmatig zand met brokken zwarte veenhoudende leem, maar weinig veenhoudend
11.50	13.00		grijs schelphoudend middelmatig zand
13.00	13.70		grijs sterk schelphoudend middelmatig zand
13.70	15.50		grijs sterk leemhoudend fijn zand
15.50	18.00		grijs sterk leemhoudend fijn zand tot zandhoudende leem
18.00	21.50		grijs sterk leemhoudend fijn zand
21.50	22.00		grijs schelphoudend middelmatig zand
22.00	24.50		grijs sterk schelphoudend grof zand
24.50	25.50		grijs leemhoudend fijn zand
25.50	26.20		grijs weinig schelphoudend fijn tot middelmatig zand
26.20	27.90		grijs weinig schelphoudend fijn zand met bovenaan sporadisch weinig leemhoudend
27.90	28.20		grijs schelphoudend fijn zand
28.20	32.20		grijs leemhoudend fijn zand tot zandhoudende leem

Informele stratigrafie - 25/10/1993

Auteur(s): Van Houtte, E. (Universiteit Gent (UGent)) Betrouwbaarheid: goed

Van(m)	Tot(m)	Beschrijving
0.00	32.20	Quartair

Figure 33. Borehole log at WP6

APPENDIX C

TRANSLATION OF BOREHOLE LOG

Table 6. Soil Profile information at WP_6 obtained from borehole measurement after translation from the original report (figure 33)

Depth(m)		Elevation(mTAW)		K_x	K_y	K_z	Sy	Porosity
From	To	From	To					
0	7.5	6.1	-0.9	20	20	2	0.26	0.43
7.5	13.7	-0.9	-7.9	40	40	4	0.28	0.39
13.7	21.5	-7.9	-14.9	0.5	0.5	0.05	0.25	0.44
21.5	22	-14.9	-15.9	40	40	4	0.28	0.39
22	24.5	-15.9	-17.9	50	50	5	0.27	0.39
24.5	25.5	-17.9	-18.9	0.5	0.5	0.05	0.25	0.44
25.5	26.2	-18.9	-19.9	25	25	2.5	0.26	0.41
26.2	27.9	-19.9	-21.9	0.5	0.5	0.05	0.25	0.44
27.9	28.2	-21.9	-22.9	17	17	1.7	0.26	0.43
28.2	32.2	-22.9	-24.9	0.5	0.5	0.05	0.25	0.44